A NOVEL REVERSING FLOW DIRECTION COLUMN TO STUDY REACTIVE FLOW AND TRANSPORT IN MIXING ZONES OF DISPARATE WATER CHEMISTRIES

A Thesis

by

REID EZEKIEL BUSKIRK

Submitted to the Office of Graduate and Professional Studies of
Texas A&M University
in partial fulfillment of the requirements for the degree of

MASTERS OF SCIENCE

Chair of Committee,	Peter S K Knappett
Committee Members,	Youjun Deng
	Franco Marcantonio
Head of Department,	Julie Newman

December 2021

Major Subject: Geology

ABSTRACT

The coupled processes of biogeochemical and hydrological processes in hyporheic zones (HZ) commonly determine the fate of contaminants in both groundwater and surface water. Many parts of the HZ experience both transient and bidirectional flow owing to hydraulic gradients created by the pairing of rapidly changing river stage with relatively steady groundwater tables. The specific contributions of end-member chemistries of the river and groundwater, and the periodicity of the river stage fluctuation, on the fate of a groundwater or river water contaminant is difficult to tease out empirically owing to laborious field conditions. Recently developed bidirectional flow column experiments offer a solution. No published studies, however, have ramped flow up and down smoothly as happens in natural riverbanks under the influence of daily ocean tides and dam releases, as well as sporadic or seasonal floods. Therefore, transient flow, bidirectional column experiments are necessary to accurate simulate how paired river water stage fluctuations and river and groundwater chemistry impact determine the fate of a contaminant within a watershed.

The objective of this project was to construct a programmable transient and reversing flow column experiment apparatus (R1D) that can mimic mixing in a sediment column between two reservoirs of disparate chemistries under a flow regime analogous to a semi-diurnal tidal sequence. To validate this device, once constructed, breakthrough curves (BTC) of a conservative NaCl tracer were compared for an experiment under reversing flow conditions using constant flux conditions and variable (sine wave) flux conditions. Calculated Peclet numbers indicated that mechanical dispersion (dispersivity) dominated over molecular diffusion. The dispersivity of the BTC were fitted to a 1-D numerical model in order to discern whether fitted dispersivity was dependent on the flow direction. Dispersivity did not change with flow

direction which demonstrates homogeneous packing of the sand column. The average linear velocities fitted to the BTC were (0.025-0.091 m/d). This apparatus is well suited to investigate a number of systems of kinetically limited and equilibrium biogeochemical reactions within permeable riverbanks. One such system is the permeable natural barriers (PNRBs) along rivers flowing through deltas with anoxic shallow aquifers with high concentrations of arsenic (As). These PNRBs capture dissolve iron (Fe) as Fe-oxides and arsenic (As) bound to their surfaces from groundwater discharging to the Meghna River, however, the initial formation and fate of these deposits under seasonal fluctuations in river stage is unknown.

DEDICATION

This Thesis is dedicated to my family, as none of this would have been possible without their love and support.

ACKNOWLEDGEMENTS

I would like to thank my committee chair, Dr. Peter Knappett and my committee members Dr. Marcantonio, and Dr. Deng for their guidance and support through the course of this research project. I also would like to thank Buz Buskirk, Marda Stribling, Jim Buskirk, Sean Lynch, Cass Midkiff, William Seward, Dr. Bayani Cardenas, Dr. Sugata Datta, Dr. Harshad Kulkarni, Dr. Kimberly Meyers, Dr. Hongbin Zhan, Kowe Carmichael, Aaron Pena Rodriguez, Selsey Stribling, Yibin Huang, Laura Rodriguez Lozada, the Chemistry Department Machine Shop and many others for their advice, support, and assistance.

I wish to thank my fellow graduate and undergraduate students for your assistance, support, and for the great times so far at A&M.

Last but certainly not least, I would like to specifically thank my parents for their encouragement, patience, support, and love.

CONTRIBUTORS AND FUNDING SOURCES

Contributors

This work was supervised by a thesis committee consisting of Professor Peter Knappett and Professor Franco Marcantonio of the Department of Geology and Geophysics and Professor Dr. Youjun Deng of the Soil and Crop Science Department.

Funding Sources

Primary funding for this project was made possible by the National Science Foundation's (NSF) Research under Grant Program EAR-1852652.

Additional funding for apparatus parts and the in-line optical dissolved oxygen sensor system was sourced from the Gould Research Grant from the Geological Society of America (GSA) Graduate Student Research Grants Program

NOMENCLATURE

Acronyms:

18.2 MΩ Deionized Water	DI
Advection-Dispersion Equation	ADE
Ammonium	NH_4^+
Arsenic	As
Breakthrough Curve	BTC
Digital to Analog Current	DAC
Dissolved Organic Matter	DOC
Dissolved Oxygen	DO
Electrical Conductance	EC
Ganges-Brahmaputra-Meghna Delta	GMBD
Hyporheic Zone	HZ
Inner Diameter	ID
Iron	Fe
Iron (Oxy)hydroxides	Fe-Oxides
Modular Three-Dimensional Finite-Difference Groundwater Flow Model	MODFLOW
Nitrate	NO_3^-
Oxidation-Reduction Potential	ORP
Permeable Natural Reactive Barrier	PNRB
Reversible Constant Flux Experiment	CF
Reversible Variable Flux Experiment	VF
Reversing Constant Flux Experiment	RCF
Reversing Flow Column Experiment Apparatus	R1D
Reversing Variable Flux Experiment	RVF
Rotations Per Minute	RPM
Sodium Chloride	NaCl

Symbols:

10^{th} Percentile Grain Size Diameter	d_{10} (µm)
60^{th} Percentile Grain Size Diameter	d_{60} (µm)
Arduino Input 12-bit Value	B
Average Grain Size Diameter	d_{AVG} (µm)
Average Linear Velocity	v (m/d)
Bulk Density	ρ_b (g/ml)
Bulk Porosity	n
Column Length	L (m)
Darcy Flux	q (m/d)
Diffusion Coefficient	D_d
Dispersivity	α (m)
Distance From Column Influent End	x (m)
Dry Mass	m_{sand}
Effective Diffusion	D*
Effective Porosity	n_e
Fitted Amplitude	F

Head Difference	dh (m)
Hydraulic Conductivity	K (m/d)
Interval Timestep	i
Longitudinal Dispersion	D_L (m^2/d)
Median Grain Size Diameter	d_{50} (μm)
Peclet Number	P
Porosity	n
Pump Calibration Best-Fits Slope	m
Pump Calibration Y-Intercept	b
Sediment Density	ρ_s (g/ml)
Tortuosity	ω
Total Sand and Water Volume	V_{total} (ml)
Total Sand Volume	V_{total} (ml)
Uniformity Coefficient	U
Volumetric Darcy Flux	Q (m^3/d)
Water Volume	V_{water} (ml)

Units:

Concentration	C/C_o
Distance	m
Normalized Concentration	C/Co
Pore Volumes	PV
Time	s
Volts	V

TABLE OF CONTENTS

Page

ABSTRACT ii

DEDICATION iii

ACKNOWLEDGEMENTS iv

CONTRIBUTORS AND FUNDING SOURCES v

NOMENCLATURE vi

TABLE OF CONTENTS ix

LIST OF FIGURES x

1. INTRODUCTION 1

2. METHODS 5

- 2.1 R1D Electronics and Plumbing 6
- 2.2 Peristaltic Pump Calibration 7
- 2.3 Accuracy and Precision of Volumetric Fluxes used in Column Experiments 8
- 2.4 In-Line Water Quality Probes 9
- 2.5 Packed Sand Column Preparation 10
- 2.6 Conservative Tracer Experiments 12
- 2.6 Numerical Modeling of Advective and Dispersive Transport and Mixing 15

3. RESULTS 18

- 3.1 Precision and Accuracy of Volumetric Flux 18
- 3.2 In-Line Probes Measuring Chemical Parameters 18
- 3.3 Conservative Tracer Breakthrough Curves 22
- 3.4 Numerical Modeling Results 24

4. DISCUSSION 27

- 4.1 Apparatus Accuracy and Precision 27
- 4.2 AGW and ASW Breakthrough Curves 27
- 4.3 Numerical Model Results 32
- 4.4 Broader Applications of Experimental Hydro-biogeochemistry 33

5. CONCLUSIONS 40

REFERENCES 41

APPENDIX A 48

APPENDIX B 50

APPENDIX C 73

APPENDIX D 76

LIST OF FIGURES

FIGURE		Page
1	Conceptual R1D Apparatus Figure	4
2	Photographs of the R1D Apparatus	6
3	Conceptual Figure of R1D Constant and Variable Flux Regimes	14
4	Conceptual Sketch of MODFLOW Model	16
5	Reversible Constant Flux (RCF) In-Line Probe Output	20
6	Reversible Variable Flux (RVF) In-Line Probe Output	21
7	Overlaid RCF and RVF EC Breakthrough curves for handheld and In-Line Probes	23
8	Overlaid RCF and RVF MODFLOW Model Breakthrough Curves	26

1. INTRODUCTION

The coupled processes of biogeochemical and hydrological processes in hyporheic zones (HZ) determine the fate of many contaminants. Mixing between oxidized river water and reducing groundwater forms hyporheic zones (HZs) whose size is mainly controlled by the hydraulic conductivity (K) of the aquifer (Wondzell & Swanson, 1996). Oscillating river stages expand the HZ considerably and drives bidirectional flow (Butturini et al., 2002; Duff & Triska, 2000). This flow switches directions at periods that are characteristic to the hydrological process driving the river stage fluctuation. These hydrological processes include: 1) semi-diurnal (12 hour) and neap-spring (14 day) ocean tides (Bianchin et al., 2010; Bianchin et al., 2011; Musial et al., 2016; Westbrook et al., 2005); 2) diurnal dam releases for electricity generation, termed "hydropeaking" (McManamay et al., 2016; Sawyer et al., 2009); and 3) seasonal fluctuations in rainfall amounts such as in monsoonal climates (Brooks & Lemon, 2007) and temperate regions impacted by spring snow melt (Ellis et al., 1998; Galler & Allison, 2008). This switching in flow direction is hereinafter referred to as a riverbank redox cycle.

These riverbank redox cycles are important for controlling solute transport and sediment-water interactions in the HZ. For example, along the Meghna River in Bangladesh, this redox cycle is driven by upstream tidal propagation from the Bay of Bengal. It may drive oxygen into riverbanks and driving the oxidation of dissolved Fe(II) to Fe(III)-oxides which the sequesters geogenic groundwater As. These are the so-called Permeable Natural Reactive Barriers (PNRB) (Berube et al., 2018; Datta et al., 2009).

The transient, bidirectional flow behavior and complex sediment-water interactions HZs are challenging to study empirically. Bidirectional flow column experiments have recently been used to investigate some biogeochemical processes (Li et al., 2020; Liu et al., 2017). To the

author's knowledge, however, only two studies that feature bidirectional column experiments applied to investigate biogeochemical processes in HZs have been published. Both studies utilized constant fluxes. No studies appear to have utilized a column experiment that ramps flow up and down smoothly in a variable flux regime as would be anticipated for a real-world site. To perform a variable flux experiment an apparatus is needed to control both the direction and magnitude of fluxes. An apparatus that can ramp up and down flow would be a more accurate simulation of real-world HZ flow regimes, and allow the experimenter to simulate riverbanks with different aquifer and river water chemistries and river stage periodicities from rivers around the world today, through deep geologic time (i.e., paleohydrology), and unravel the recent past and future impacts of artificial river stage regulation as 60% of the world's rivers are dammed (McManamay et al., 2016).

The objectives and hypotheses of this study are to:

1. construct a novel automated 1-D transient and reversing flux column apparatus to simulate saturated bi-directional flow regimes in HZs;
2. verify the apparatus can simulate complex transient flow regimes by comparing transport of a conservative tracer during a reversing constant flux (RCF) and reversing variable flux (RVF) experiment. It is hypothesized (H1) that the transport of the conservative tracer in these two experiments will result in identical breakthrough curves (BTCs) since transport is controlled by advection and mechanical dispersion (i.e., dispersivity).
3. determine whether sediment dispersivity is direction-dependent and stable over time. It is hypothesized (H2) that modeled sediment dispersivity will be direction-independent for a well-packed homogenous sediment column. Deviations in

dispersivity over time, if present, would be due to sediment compaction over the course of the experiment or preferential flow pathways that open and shut when flow is reversed.

If these conservative tracer tests are successful, then this device is ready for use to isolate the respective roles of flow and reaction kinetics in biogeochemical reactions such as those responsible for PNRB formation.

This study will utilize a reversing flow direction 1-D column apparatus (R1D) to simulate the tidally mediated flow reversals observed at a known PNRB site along the Meghna River (Berube et al., 2018) (Fig. 1). To achieve this, the R1D was programmed to open and shut a series of valves and start and stop two independent peristaltic pumps that injected AGW and ASW into opposing ends of the column. The AGW was characterized by high total dissolved solids (TDS) consisting of sodium chloride (NaCl) and the ASW was DI water. In-line electrical conductance (EC) monitored the effluent from the column to determine the proportions of groundwater and surface water exiting the column.

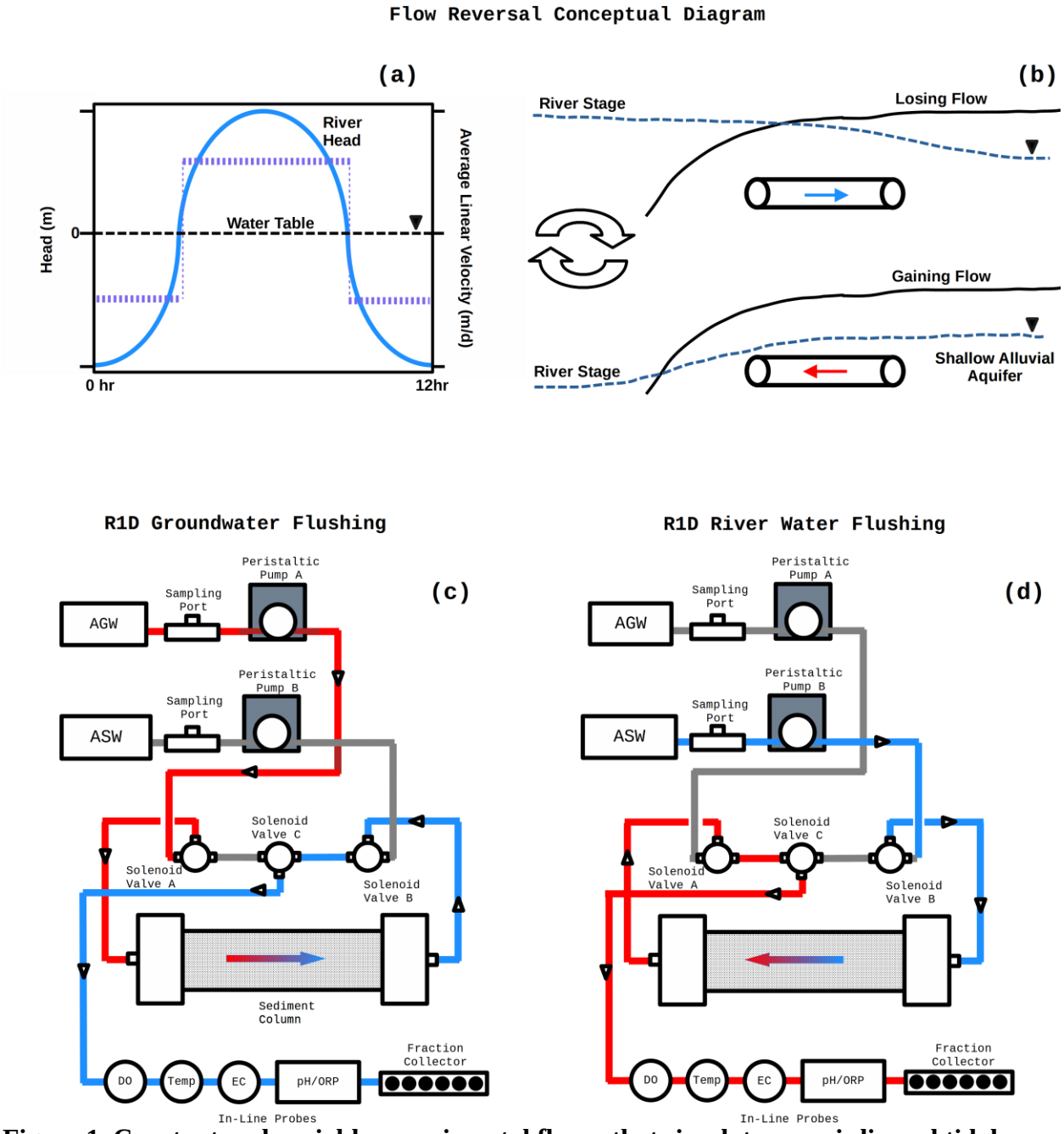

Figure 1. Constant and variable experimental fluxes that simulate a semi-diurnal tidal cycle (a). A conceptual sketch of transient flow reversals that the device was designed to simulate is presented (b). Schematic diagram of the plumbing connections, valves, pumps and in-line probes (c-d). After the artificial groundwater (AGW) is flushed through the sediment column (c), the valves are switched, the AGW pump (Pump A) is turned off, the ASW pump (Pump B) is turned on, causing the artificial surface water (ASW) to be flushed out of the column from the opposite direction (d). This cycle is repeated periodically (a) using an abrupt constant flux reversal (dashed-purple) or with a sine wave (solid-blue) to mimic real-world flux regimes.

2. METHODS

A physical model of a bi-directional flow in a riverbank requires reversing flux conditions to mix the groundwater and river water end-members (Figs. 1-2). The physical model that was developed is a reversing flux, 1-D column apparatus that alternately flushes water through opposing ends of a sediment column at timed intervals. This apparatus was designed and built since a comparable apparatus was not available commercially, and few examples exist in the literature (Bear, 1961; Li et al., 2020; Liu et al., 2017). The experiments conducted by Bear (1961), Liu et al. (2017), and Li et al. (2020) used simple manual setups. Automating the flux regimes permits long-term operation of the experiment over many flux-reversing cycles which accurately mimics a coastal river stage fluctuating under the influence of ocean tides (Berube et al., 2018), as well as day-time water releases by hydroelectric dams to meet higher day-time electricity demands (Fritz & Arntzen, 2007; Sawyer et al., 2009). The design included measuring physical and chemical parameters (i.e., temperature, pH, electrical conductance (EC), oxidation-reduction potential (ORP), and DO in the column effluent with in-line probes. Discrete effluent samples were collected using a commercially available fraction collector (SuperFrac, Pharmacia, Stockholm, Sweden).

The design and construction of the apparatus, and programming and calibrating the pumps and probes required most of the project's time and effort. Each individual component needed to be tested to verify it worked as intended and communicated correctly with the Arduino microcontroller. Next, all components needed to be tested while running simultaneously to ensure that the Arduino microcontroller programs could both receive data and send commands. After initial testing, individual components frequently needed to be replaced or modified during the apparatus design and construction period. The total material expenditures for the apparatus

was approximately 5,000 USD, excluding a rather expensive, but necessary optical dissolved oxygen probe (2,183 USD). The laboratory apparatus was built using readily available, affordable components. The programming was done with the free, open-source Arduino programming language.

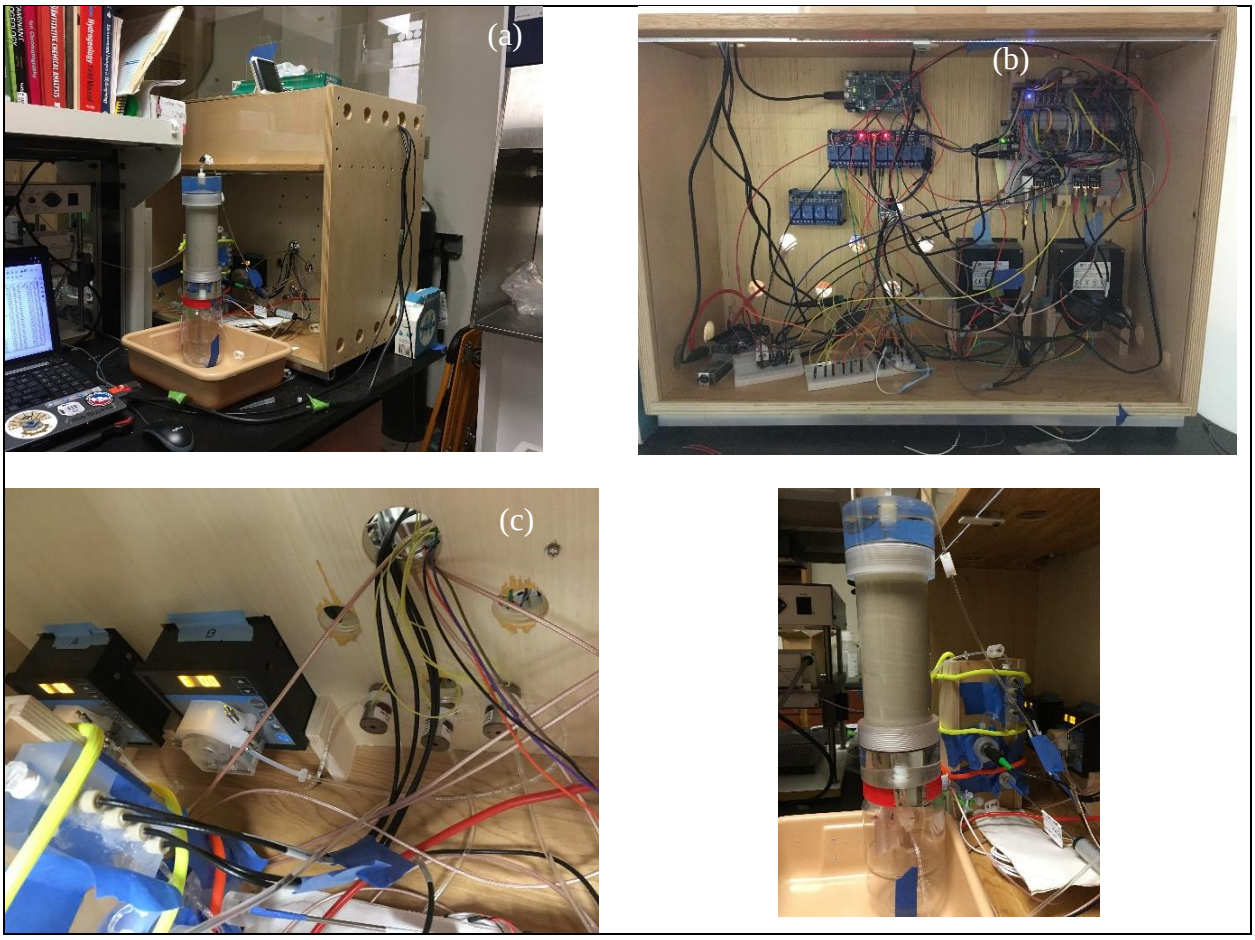

Figure 2. The completed R1D apparatus (a), electronic wiring controlling the apparatus (b), peristaltic pumps and solenoid valves (c), and row of in-line effluent probes and column (d).

2.1 R1D Electronics and Plumbing

The R1D setup utilized an Arduino Due Microcontroller to control two programmable pumps which drew water from the AGW and ASW reservoirs (Fig. 1; Fig. 2a-b). These

reservoirs are connected to the influent end of the packed sand column through two valves which are controlled by the Arduino (Fig. 1b-c; Fig. 2c-d). Every time there is a flux direction reversal, the effluent end of the column becomes the influent end. Therefore, valve C synchronizes with the two upstream valves A and B, which are located closer to the artificial end-member reservoirs to accept water that it directs to the new effluent end of the column. In-line probes measure the physical and chemical parameters continuously. These will be described in section 2.3 (Appendix A).

The Arduino Due was connected to a computer to receive programs to run the experiment and to return the following data: timestamp, pore volume (PV) estimates, and the values of the physical and chemical parameters measured by the inline probes. A PV is a dimensionless unit expressing the volume of water transported through a column relative to the total pore space volume in column sediments. The volumetric flux of two low flow (0.005-32 mL/min) variable-speed peristaltic pumps (Model BQ80S, Golander Pump, Norcross GA USA) was controlled by the digital to analog 12-bit output pin of the Arduino. The output voltage range was expanded from 0.55-2.75V to 0-3.3V using a dual power LM358 operational amplifier (LM358, Texas Instruments, Dallas TX USA). The three 12V DC polytetrafluoroethylene (PTFE) plastic body solenoid diverting valve (2552N14, McMaster Carr, Elmhurst, IL) were actuated with a relay module using an electronically isolated power source. The solenoid valves were negative voltage spike compensated with flyback diodes (Model 1N4007, Ltvystore Seattle WA USA).

2.2 Peristaltic Pump Calibration

The R1D apparatus injects water into alternating ends of the column at a programmed volumetric flux using the variable digital to analog current/voltage (DAC) pin voltage (0-5 V)

from the Arduino DAC pin. However, the relationship between input voltage based on the 12-bit value from the instrument and the volumetric water flux rate must be determined for programmed flux to be accurate. Pump revolutions per minute (RPM) could not be determined via this calibration approach. Hence, to produce accurate fluxes, the volumetric flux was manually calibrated against input voltages from the R1D via input Arduino program 12- bit value.

Calibrations were repeated periodically during the testing phase of the apparatus. These calibrations were repeated when tubing wore out or when the device was left inactive for several weeks. Different tubing sizes were tested in the pump heads to determine the range of potential volumetric fluxes. Measured volumetric flux (Q) was regressed upon the 12-bit input value (B) using linear regression to fit the slope (m) and intercept (b) in the following equation: (Appendix B)

(Eq. 1) $$Q = B * m + b$$

The calibration curves differed even for the same tubing sizes owing to slightly differing screw tightness on the pump carriage. Therefore, any change to screw tightness or when new tubing was used (even the same diameter) required recalibrating the pumps. The calibration curves were then applied to produce the specified flux for the experiments. All volumetric flux calibration measurements were performed on the complete connected system of tubing, valves and packed sand column.

2.3 Accuracy and Precision of Volumetric Fluxes used in Column Experiments

To test the precision of volumetric flux produced by the peristaltic pumps triplicate measurements were made for each voltage level (B). These calibrations were repeated several times for the same tubing diameter and carriage tightness. From these calibration measurements,

the standard errors of the calibration curve used for the experiments were calculated, and 95% confidence intervals were calculated for triplicated measurements in other calibration curves (Appendix B).

To test overall R1D flux accuracy, a water recovery estimate was performed, comparing the calculated total water of water expelled from the apparatus during the two reversible flux conservative tracer experiments and the actual amount of recovered water.

2.4 In-Line Water Quality Probes

In-line temperature, EC, pH, and ORP probes were installed in custom-made flow cells downstream of the column effluent. The EC probe was an Atlas Scientific Mini 1.0 EC probe (Mini 1.0 EC Atlas Scientific, Long Island City NY), and was two-point calibrated with 88 µS/cm (Biopharm, Hatfield AR) and 1413 µS/cm solutions (Atlas Scientific Long Island City NY USA). A Micro pH Probe (Micro pH Probe, Atlas Scientific, Long Island City NY) was calibrated at the start of the experiment using pH buffers at 4, 7, and 10 (Atlas Scientific, Long Island City NY USA). A Micro ORP Probe (Micro ORP Probe, Atlas Scientific, Long Island City NY USA) was calibrated using a 225 mV (Zobell's) solution (Atlas Scientific, Long Island City NY USA). The optical DO probe (PICO-O2, Pyroscience, Aachen, Germany) was separately controlled and its measurements were logged to a computer using an Arduino Mega (ELEGOO Mega 2560, ELEGOO, Shenzhen China). However, it was installed and tested after the RCF and RVF experiments were performed, so optical DO results are not presented.

All in-line probes were installed into custom-built acrylic flow cells with the inlet and outlet ends oriented vertically to prevent the buildup of air, which can suppress the EC signal. It is important to minimize dead volume to minimize mixing and reaction of effluent water downstream of the packed sand column. Dead volume in the flow cells with the probes installed

was 0.0161 mL for the optical DO probe flow cell, 0.275 mL for the EC probe flow cell, and 1.36 mL for the combined pH and ORP flow cell. Total dead volume for the effluent tubing and flow cells combined was 4.36 mL.

In-line temperature, DO, pH, EC, and ORP was measured at a 30 second frequency. The computer logged the probe data, which was output from the Arduino, into a comma delimited file using the software puTTY (Version 0.76) (Tatham, 2021).

Electrical conductance was used as a conservative tracer to observe the impacts of advective and dispersive mixing between the end-member solutions. To verify the EC readings reported by the inline EC probe, these were compared against those measured on grab samples from the fraction collector using a hand-held EC probe (EC 300, YSI Environmental, Yellow Springs OH) which had been calibrated with the same calibration solution as the inline probe.

2.5 Packed Sand Column Preparation

The sand column had a length of 20 cm and an inner diameter of 6.30 cm (Knappett et al., 2008). The column sand was a Graded Standard Sand (Cube Test Sand) (HM-108, Gilson Company Inc, Lewis OH USA)The median (d_{50}), tenth percentile (d_{10}) and sixtieth percentile (d_{60}) grain size diameter of the sand used were 359 µm, 190 µm, and 389 µm, respectively calculated from sieve data provided from the manufacturer (ASTM & others, 2011; Schoeneberger et al., 2012). This qualifies the sand as a medium sand, grains were well sorted and rounded (Boggs Jr, 2014). The uniformity coefficient (U) was 2.05 where:

(Eq. 2) $$U = \frac{d_{60}}{d_{10}}$$

According to the manufacturer, the grain size range of this sand extended from 149 to 1190 µm (Graded Standard Sand Model No. HM 108, Gilson Company Inc, Center OH USA). The sand was comprised of 98.7-99.9 wt% SiO_2, <1.1 wt% Al_2O_3, <0.1% FeO, and <0.1% TiO.

To improve the reproducibility between separate experiments by prevent air bubbles from being trapped in pore spaces the column was wet packed (Appendix C) (Lewis & Sjöstrom, 2010). The packing method was modified from a procedure used to pack sand columns for virus transport studies (Brush et al., 1999). Wet packing was achieved by gently pouring sand into the column that was filled with deionized (DI) water (18.2 MΩ) water. Next, the sand was consolidated by percussive tamping of the column top rim, rather than directly tamping the sand, to prevent the formation of preferential flux paths. The column was then pre-flushed with DI for 1.93 PV over 6 hr in both directions (3.86 PVs total) to flush out residual solutes and clay particles.

Based on triplicate measurements, the mean and 95% confidence interval of sediment porosity (n) and hydraulic conductivity (K) of the packed column were determined to be 0.367±0.008 and 30.0±0.08 m/d, respectively. These were determined by measuring the bulk sediment density of the saturated sand in graduated cylinders and a constant head permeameter test, respectively (Model 3891, KarolWarner, Powell OH, USA), respectively (Driscoll, 1986, p. 74; Freeze & Cherry, 1979; Weight, 2008, p. 99). The sand was packed into the graduated cylinders and the constant head permeameter using the same method that was modified from Brush et al. (1999) as used to pack the columns. The permeameter test rearranges Darcy's law to solve for hydraulic conductivity:

(Eq. 3) $$K = \frac{Q*L}{A*dh}$$

where dh is the difference in water elevation in manometers located upstream and downstream of the packed sand column, L is the length of the packed sand which was 16.0 cm, A is the cross-sectional area of the column which was 31.2 cm, and Q is volumetric flux which was measured via a graduated cylinder and stopwatch. Porosity of the packed sand was calculated using the following equations:

(Eq. 4) $$V_{sand} = V_{total} - V_{water}$$

(Eq. 5) $$\rho_s = \frac{m_{sand}}{V_{sand}}$$

(Eq. 6) $$\rho_b = \frac{m_{sand}}{V_{total}}$$

(Eq. 7) $$n = 1 - \frac{\rho_b}{\rho_s}$$

where ρ_b is the dry bulk density, ρ_s is the sediment density m_{sand} is the dry mass, V_{total} is the bulk sand volume, V_{water} volume of water, and V_{total} is the of combined sand and water in the graduated cylinder were measured directly in the lab in triplicate using three separate graduated cylinders to calculate n. The porosity obtained from this method is bulk porosity, which is assumed to be equal to effective porosity (n_e). This was used as the initial porosity in the numerical model before the manual fitting procedure was applied as described in section 2.7.

2.6 Conservative Tracer Experiments

The EC values in the column effluent were plotted against PVs to visualize the breakthrough curves (BTCs) of both end-member waters for the RCF and RVF experiments. Both the RCF and RVF experiments were run for 24 hr. The RCF experiment was run first, and the RVF experiment was performed immediately afterwards using the same volumetric flux calibration curve which was measured prior to the first experiment. During this time there were

four 6 hr cycles (three reversal events). In each 6 hr cycle 1.93 PV of either AGW or ASW was injected into opposing ends of the column. This resulted in a total of 7.72 PV injected over the course of the experiment. During the first and third cycles, AGW (580 mg/L NaCl) was injected. During the second and fourth cycles, ASW (DI water) was injected into the opposite end of the column.

Figure 3 presents the flux regimes used in the column experiments. During the RCF experiment, the magnitude of the volumetric flux was maintained at 1.24 mL/min (Fig. 3a). In contrast, during each 6 hr interval during the RVF experiment, the magnitude of volumetric flux was ramped up and down by changing Q every 30 seconds to approximate a sine wave over 0.0544 to 2.01 mL/min (Fig. 3b). To achieve 1.93 PV injection per 6 hr cycle, the necessary input voltage (B) was calculated using the following equations:

(Eq. 8) $$\mathrm{Q}_i = \mathrm{F} * \sin(\pi \frac{\mathrm{i}}{720})$$

(Eq. 9) $$\mathrm{Bit}_i = \frac{\mathrm{Q}_i - \mathrm{b}}{\mathrm{m}}$$

(Eq. 10) $$\mathrm{V}_i = 0.5 * \frac{\mathrm{Q}_i - \mathrm{b}}{\mathrm{m}}$$

where F is the fitted maximum amplitude of the sine wave and i is the 30 second interval step in the 6 hr cycle. The predicted flux using an estimated F in (Eq. 8) and the parameters m and b from the pump calibration curve, were used to calculate the corresponding input bit value (voltage) in (Eq. 9). The calculated volume of water for each 30 second step was summed for all 720 steps in the cycle and compared against the estimated column pore volume based on porosity (1848 mL). Assuming a porosity of 0.37 (based on the measurement of porosity in graduated cylinders) each PV was 462 mL, therefore four cycles required 1848 mL of AGW or ASW. The

maximum amplitude value was then manually adjusted until the sum of the estimated 720 step volumes fitted the 24 hr experiment water volume exactly.

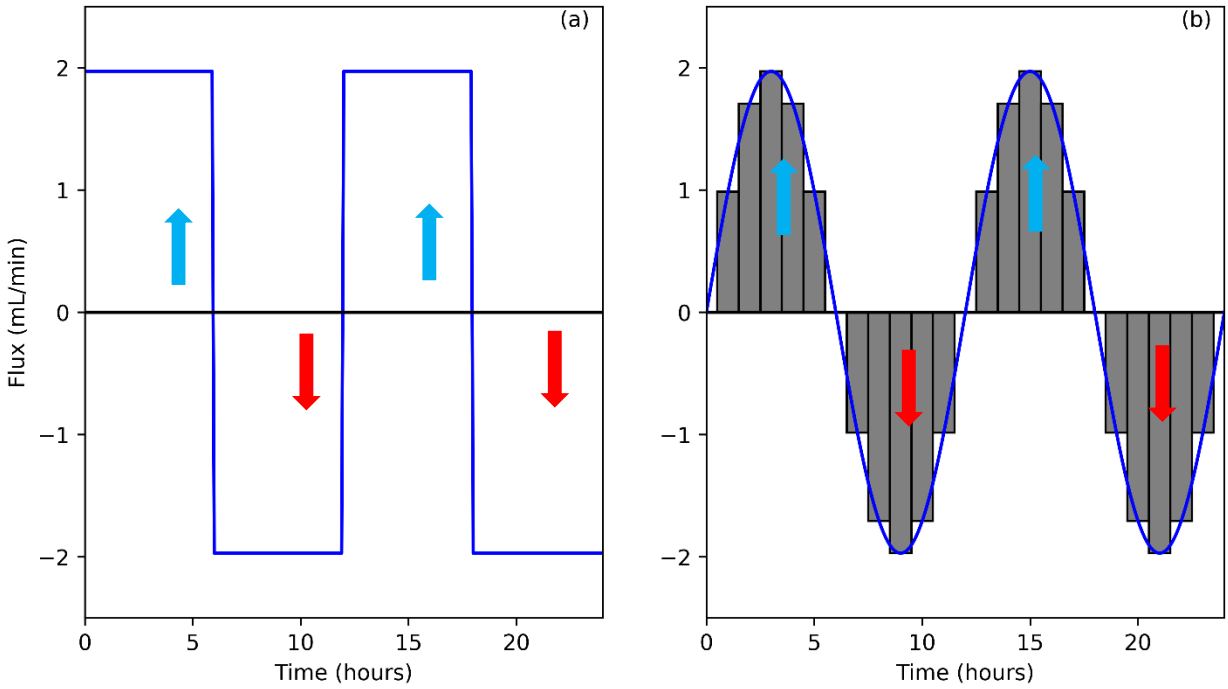

Figure 3. Conceptual flux regimes applied in the R1D apparatus. Reversing constant flux (a) and variable flux (b) experiments. The variable flux experiment consists of 720 boxes—the five presented boxes per 6 hr cycle are for demonstration purposes.

The AGW had a conductance of 1,832±2 µS/cm EC, based on five replicate samples. This was created by dissolving 17.534 g of NaCl (Sodium Chloride ACS (12314, Alfa Aesar, Ward Hill MA USA) in 30 L of 18.2 MΩ DI water. The ASW consisted of 18.2 MΩ DI water with an EC of 0.5±0.1 µS/cm, based on five replicate samples. The sodium and chloride ions were assumed to not interact with the quartz sand. Conservative NaCl is an appropriate assumption given the column matrix is quartz sand. The classic column experiment by Bear utilized a quartz sand matrix and EC as a conservative tracer in a reversing flow apparatus (Bear, 1961).

Effluent samples were collected in 15 mL falcon tubes using the fraction collector. Samples were collected at twelve and eight minute intervals during the RCF and RVF experiments, respectively. The accuracy of the estimated volumetric fluxes from the calibrated peristaltic pumps during each experiment was assessed by comparing the predicted volume against the summed weights of all samples. Water density was assumed to be 1 g/mL irrespective of EC.

2.7 Numerical Modeling of Advective and Dispersive Transport and Mixing

We utilized a numerical model to simulate the conservative transport of EC with the Advection-Dispersion Equation (ADE). This model was used to estimate effective porosity (n_e) and dispersivity (α). This model represents a first step toward a more sophisticated reactive flow and transport model for fitting kinetic and thermodynamic equilibrium terms for a specific system of reactions such as the formation of a PNRB and As sorption to it. Such a model will be necessary to isolate specific physical and chemical processes, such as adsorption of solutes on the column matrix and to explore the interaction between pore-water residence times and reaction kinetics (Gu et al., 2007).

Visual MODFLOW (Visual MODFLOW 4.6.0.169, Waterloo Hydrogeologic, Waterloo ON, Canada) was used to fit the ADE to the observed conservative BTC (Harbaugh et al., 2000) (Eq. 11)

(Eq. 11) $$D_L \frac{\partial^2 C}{\partial x^2} - v\frac{\partial C}{\partial x} = \frac{\partial C}{\partial t}$$

(Eq. 12) $$D_L = \alpha v + D^*$$

(Eq. 13) $$D^* = \omega D_d$$

(Eq. 14) $$v = \frac{q}{n_e}$$

where D_L is longitudinal hydrodynamic dispersion, C is concentration, x is the distance from the influent end of the column, v is average linear velocity, D* is effective diffusion, D_d is the coefficient of molecular diffusion, t is time, and ω is the value of tortuosity for the sand. Longitudinal hydrodynamic dispersion is the rate solutes mix along a flow path due to coupled processes of mechanical flow dispersion and molecular diffusion. Mechanical flow dispersion (α*v) is dependent on the average linear velocity of the solute particles and dispersivity, which is a coefficient specific to the column matrix. Effective diffusion is the rate which solute particles move through the column via diffusion, and this term takes sediment tortuosity into account since it slows the rate of diffusion. It is assumed that D_d for EC in the model is ($1.44*10^{-4}$ m^2/d). This number is the arithmetic average of D_d for Na^+ ($1.15*10^{-4}$ m^2/d) and Cl^- ($1.75*10^{-4}$ m^2/d) which are constant for marine waters and pore-waters within saturated sediments (Yuan-Hui & Gregory, 1974). Tortuosity was assumed to be 0.7, based on prior column experiment studies (Fetter et al., 1999; Perkins & Johnston, 1963). Before fitting, the initial values of α, n_e, and K were set to 0.0001 m, 0.37, and 3.47×10^{-4}m/s (30.0 m/d), respectively.

The software MODFLOW solves the ADE equation (Eq. 11) using a finite difference scheme under steady-state or transient flux conditions (Harbaugh et al., 2000). Rather than simulating a cylindrical column, a rectangular box was simulated with the same cross-sectional area. It had a length and height of 0.204 and 0.056 m, respectively (Fig. 4). Initial water head was set to 0.0558 m in the cells.

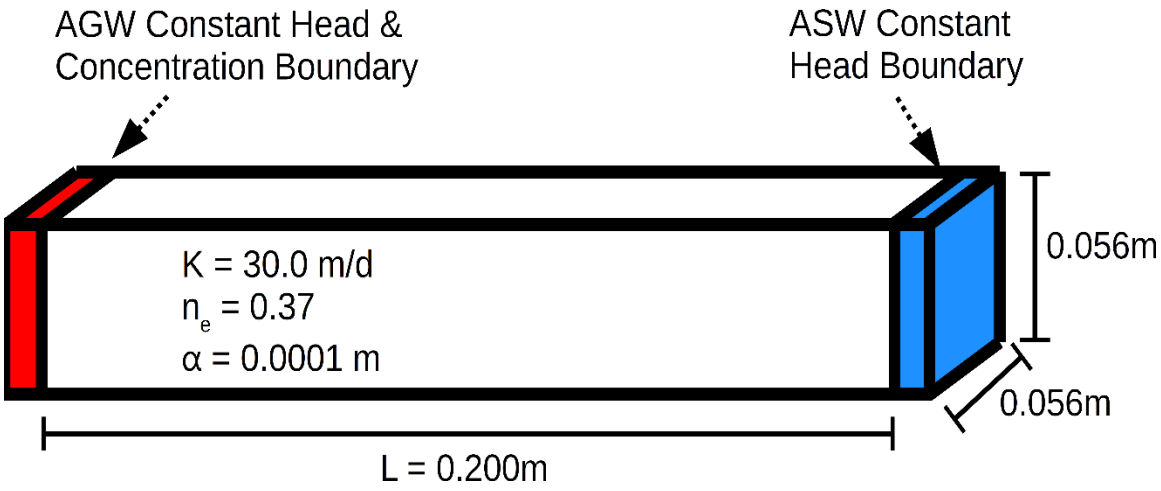

Figure 4. Dimensions of the model including the boundary conditions and hydraulic parameters for the sand used in the R1D experiment and initially entered into the MODFLOW model.

Influent water flux from the AGW and ASW reservoirs were simulated using a set of constant head boundaries on the leftmost cell of the column for groundwater and the rightmost cell of the column for river water. Constant head boundary was chosen since Visual MODFLOW does not have the option to simulate variable flux boundaries. Volumetric flux from the RCF and RVF experiments, the sand K, and the column dimensions were used to calculate the heads at the AGW and ASW ends of the model. In the model, a constant concentration boundary was placed at the leftmost cell to correspond with the inflow of AGW. To simulate ASW water inflow, the rightmost cell of the column was not assigned a constant concentration boundary which effectively gives the influent from the right a tracer concentration of zero.

The model was manually fit with respect to n_e and α. It is important to recognize that Visual MODFLOW cannot be directly fitted for v, but v is implicitly fitted when n_e is fit to the data (Eq. 11). The resulting v was then used to calculate the Peclet numbers (Eq. 15) during the RCF experiment using the following (Cushman & Tartakovsky, 2016):

(Eq. 15) $$P = \frac{v*L}{D_L}$$

where L is the length of the column. The model was first fit to the RCF observations since this data represents the simplest flow scenario, and the resulting fitted n_e and α were used as input for the RVF observations. At higher advective velocities, mechanical dispersion ($v\alpha$) dominates over diffusion (D*). Mechanical dispersion is distance-dependent, rather than time-dependent. Therefore, the modeled breakthrough curves should be the same for both the RCF and RVF experiments.

3. RESULTS

3.1 Precision and Accuracy of Volumetric Flux

The precision, represented by the standard error of the calibration curves of the groundwater and surface water pumps were 0.0186 mL and 0.0122 mL, respectively. A total of 94.9% and 95.1% of the water that was predicted to have flown through the column was physically recovered by weighing from the RCF and RVF experiments, respectively.

3.2 In-line Probes Measuring Chemical Parameters

The computer recorded continuous logs of temperature, EC, pH and ORP measured by the in-line probes receiving the column effluent for both RCF and RVF experiment (Figs. 5-6). Volumetric flux throughout the experiment was presented to provide context for the physical and chemical parameter values. The breakthroughs of EC (Figs. 5a, 6a) will be described in detail in the following section (3.5) for both experiments. Temperature in the lab remained stable between 21.49 to 22.40 °C for both the RCF and 21.34 to 22.76 °C for VRF experiments (Figs. 5b, 6b). Effluent pH rapidly dropped to 3-4 when AGW was displacing ASW from the column. This unusually low pH behavior was likely due to the pH probe malfunctioning due to operating past its life expectancy. Subsequently, effluent pH rose to 6 as ASW displaced AGW. The same behavior in pH was observed in both the RCF and RVF experiments. Effluent ORP remained stable at approximately 319 mV for both experiments.

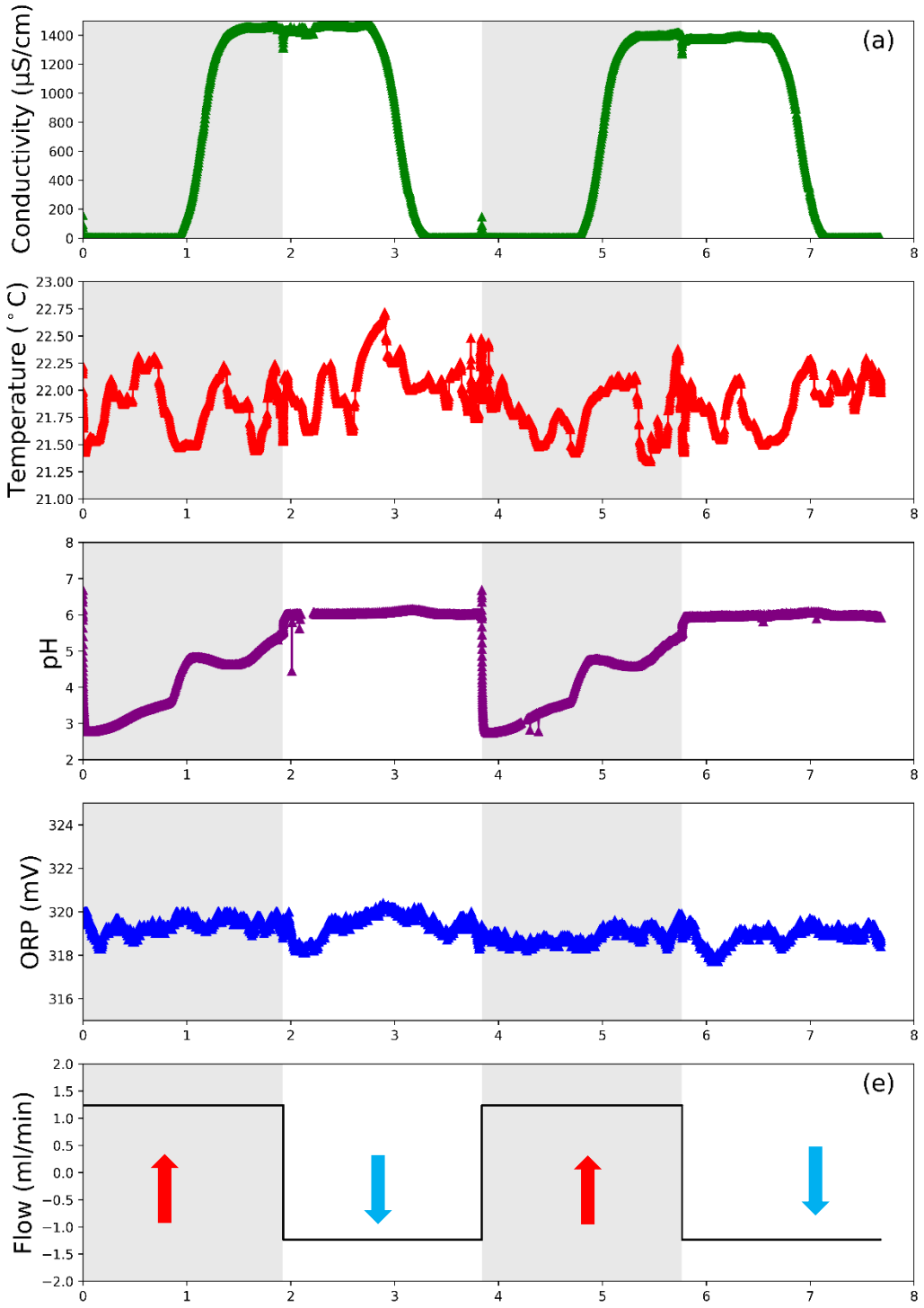

Figure 5. This figure presents EC (a), temperature (b), pH (c), ORP (d), and direction of volumetric flux (e) for the RCF experiment. Grey and white regions indicate flux reversal periods and direction. In panel (e) red and blue arrows correspond to periods when AGW (580 mg/L NaCl) and ASW (DI) were injected into the column, respectively.

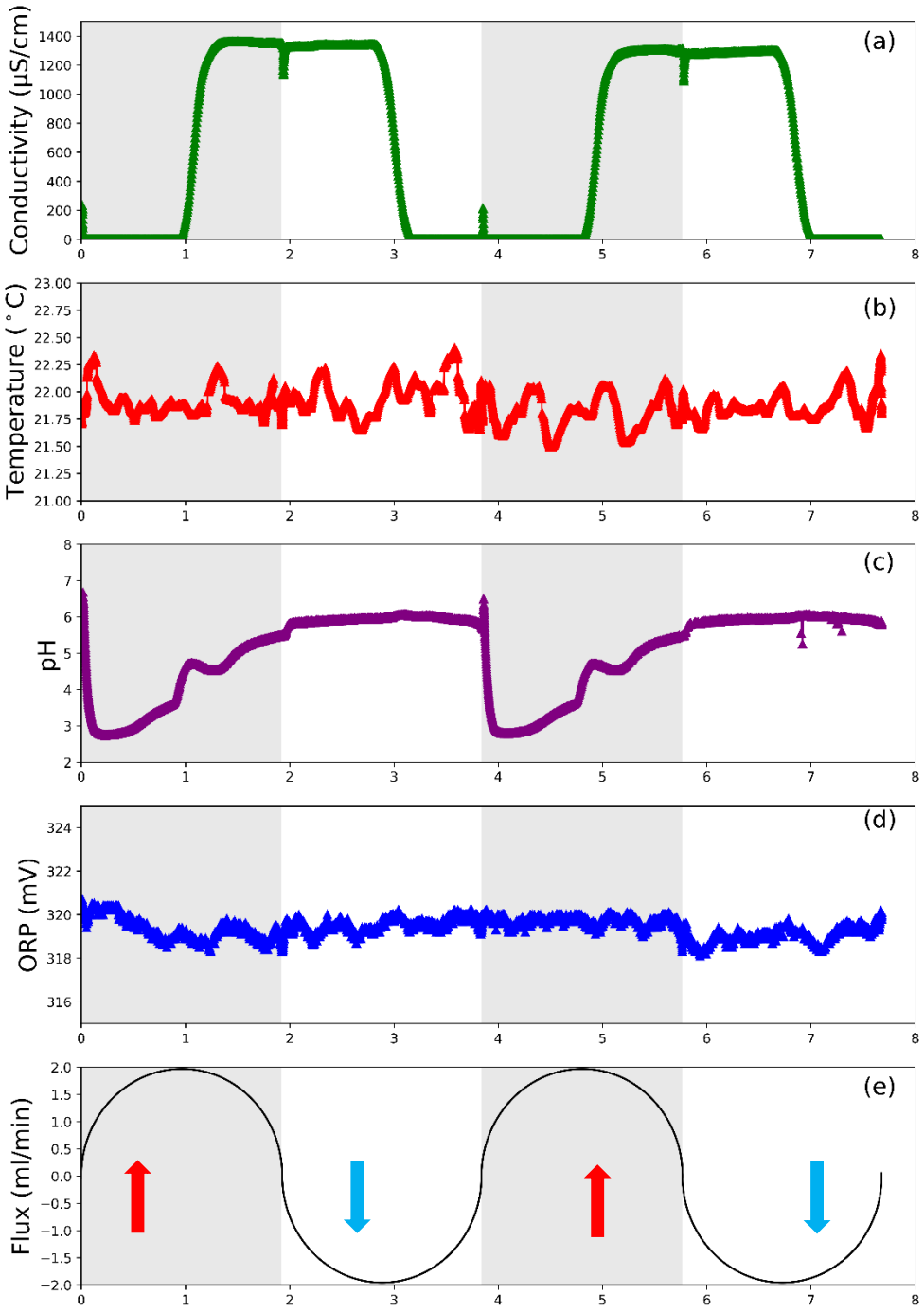

Figure 6. This figure presents EC (a), temperature (b), pH (c), ORP (d), and direction of volumetric flux (e) for the RVF experiment. Grey and white regions indicate flux reversal periods and direction. In panel (e) red and blue arrows correspond to periods when AGW (580 mg/L NaCl) and ASW (DI) were injected into the column, respectively.

3.3 Conservative Tracer Breakthrough Curves

Both the in-line probe and fraction collector samples show very similar EC BTCs for both the RCF and RVF experiments (Fig. 7). The observed increase in EC during the first and third flushing cycles with AGW water correspond to the AGW displacing the ASW from the column. This corresponds to an ebb tide when AGW displaces fresh river water from a riverbank aquifer.

This ebb tide, high EC breakthrough was characterized by three features; 1) an initial EC instrument artifact spike (0-0.05 C/C_o) which occurs immediately after pumps are turned on and begin pumping water through the column (Fig. 7). This was due to flushing a length (8.5 cm) of tubing connecting solenoid valves A and C (grey tube in Figure 1) which trapped a small volume (0.17 mL) of the AGW solution. The small volume of AGW that was flushed out of this tubing section causes the brief 0.01 PV (2.31 mL) EC spike.; 2) Next, EC remains at a 0.0 C/C_o baseline for approximately 1 PV; 3) Lastly, at 1 PV, the rising limb of the BTC begins which rises to approximately the influent concentration (C/C_o =1). The width of the rising limb of the BTC is approximately 0.5 PV.

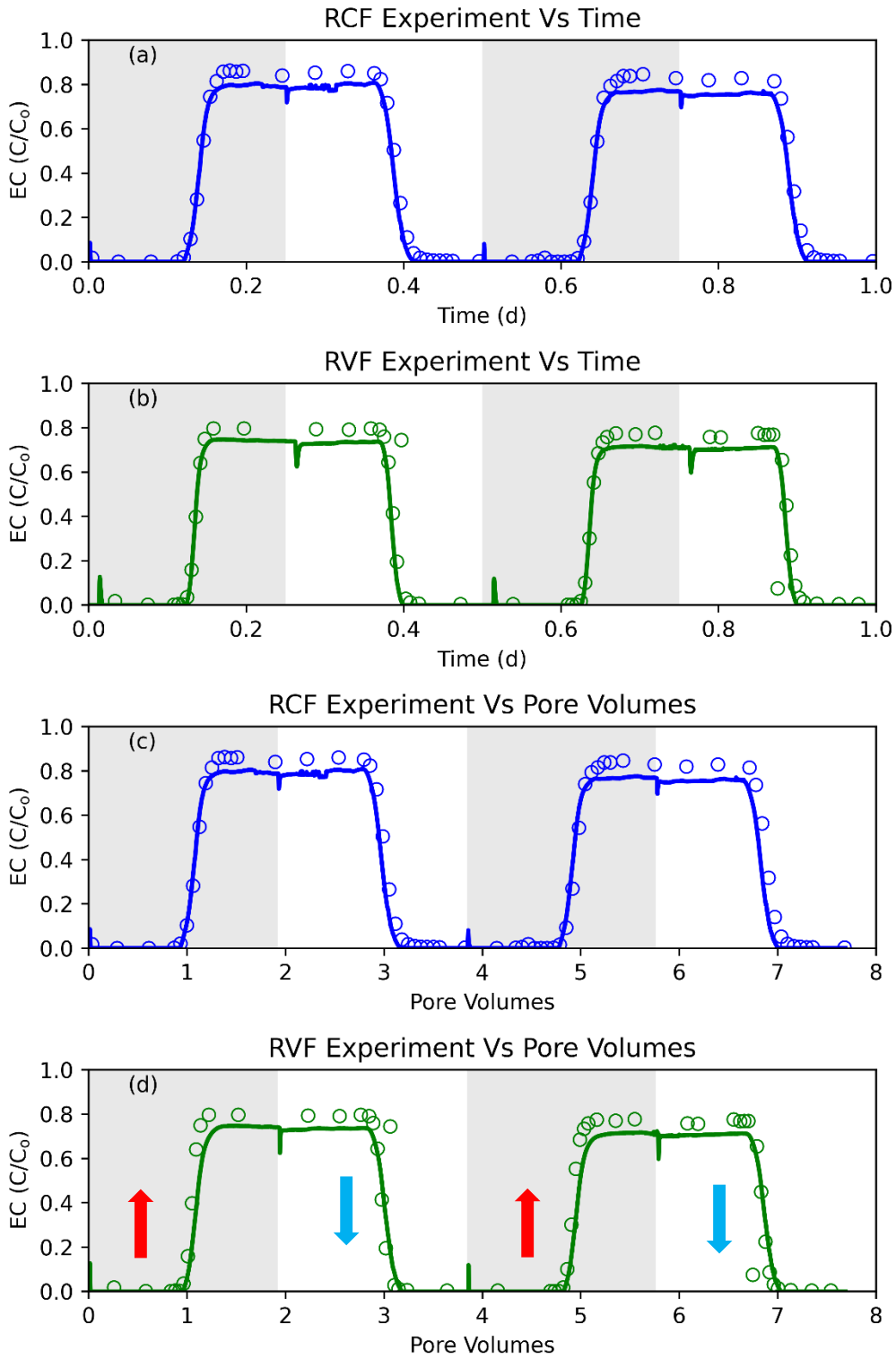

Figure 7. Uncorrected BTC of normalized EC from the column experiment for the RCF (blue) and RVF (green) experiments using fraction collector samples and the in-line probe. In panel (d) red and blue arrows correspond to periods when AGW (580 mg/L NaCl) and ASW (DI) were injected into the column, respectively.

Then, during the second (1.92-3.84 PV) and fourth (5.76-7.68 PV) cycles following the 6 hr AGW cycles the column is flushed with ASW from the opposite direction. This mimics river water entering a riverbank aquifer under rising tide conditions, displacing the high EC groundwater. The BTC breakthrough of high EC AGW that is initially expelled from the column mimics water flowing back into the riverbank. The features of the rising tide BTC is: 1) a brief drop in EC owing to DI water trapped in the tubing between valves A and C (see grey line in Figure 1c-d); 2) a plateau in EC near the AGW end-member EC ($C/C_o = 1$) while AGW was expelled; 3) a falling limb which is the start of the BTC of ASW.

The four BTC's (two rising limbs and two falling limbs) are nearly identical in both the RCF and RVF experiments regardless of whether EC is plotted against PV or time (Fig. 7). One consistent feature was that the peak EC measured on the effluent in both the in-line probes and on discrete samples had only 80% of the 1823 µS/cm (C_o) in EC that was measured in the AGW reservoir. The top of the plateau should correspond to $C/C_o=1$. The fact that an upper EC plateau is reached in each cycle demonstrates that the AGW has passed all the way through the column despite having only 80% of the expected EC signal. This drop in EC signal appears to be an artifact of how the in-line and handheld EC probes were calibrated. For this study, the data was renormalized to the maximum value of the EC breakthrough curves to permit a direct comparison to the model.

3.4 Numerical Modeling Results

The fit of the numerical model to the renormalized observed BTC's of the RCF and RVF experiments are presented in Figure 8. The fit was performed via manual calibration to the observed R1D data since the MODFLOW parameter calibration software does not permit the

numerical optimization of n_e or α for a transient model. In general, the model matches the observed BTCs in the RCF experiment with the exception of the initial EC spike when the pumps are switched (Fig. 1). The fitted n_e and α were 0.41 and 0.0003 m, respectively for the RCF experiment. the corresponding Peclet number was 537 from the RCF. In contrast the Peclet number ranged from 103-579 in the RVF experiment using the lowest and highest fitted values of v (Fig. 8a). To test H1, the RVF model was simulated using the fitted n_e and α from the RCF model. Applying the same values of n_e and α as the RCF model to the predicted BTCs for the RVF model were delayed in PV space (offset to the right) from the observed EC values (Fig. 8b).

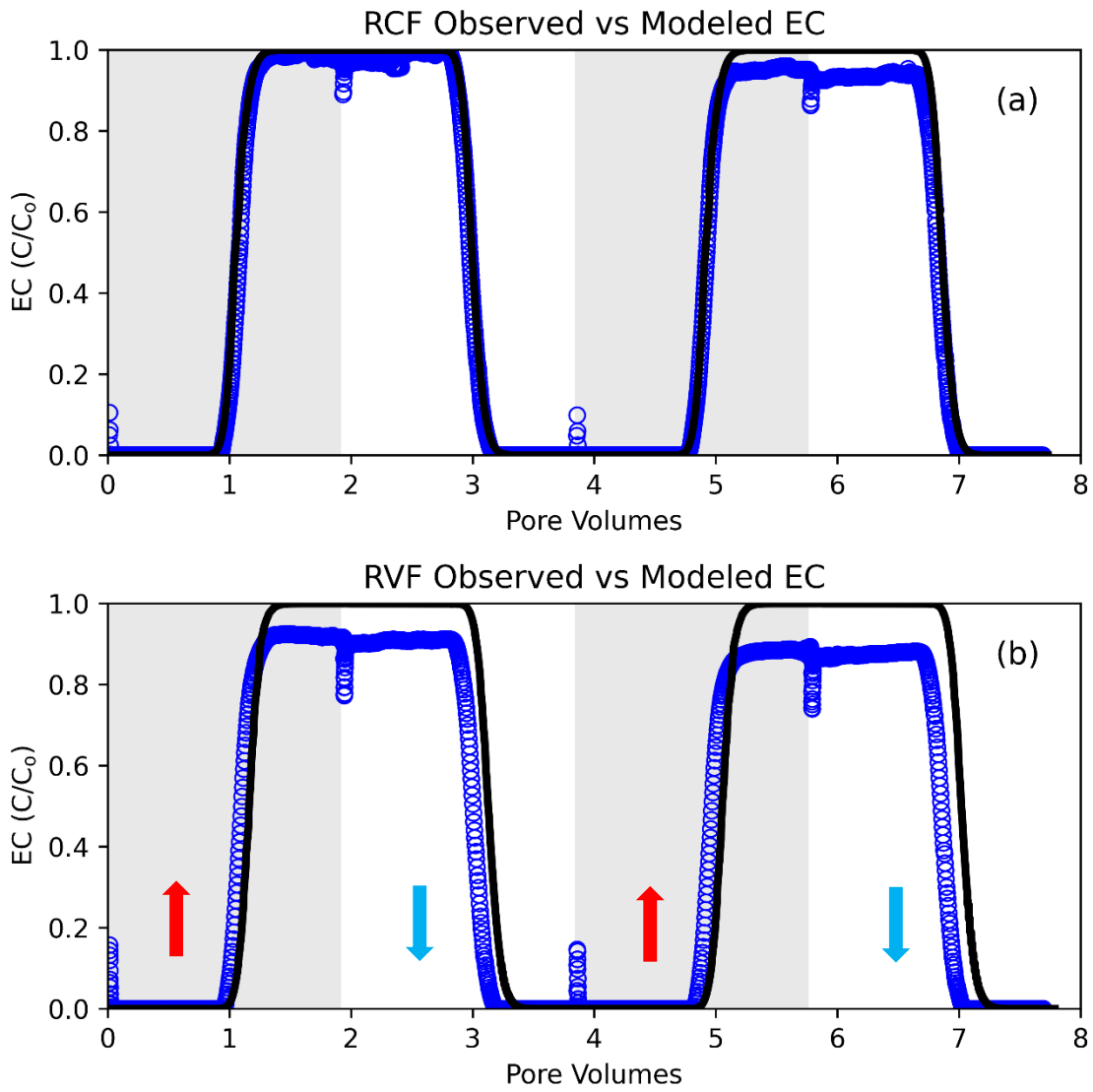

Figure 8. The fitted MODFLOW model (black line) compared to observed EC values from the in-line probe (blue circles) for the 24 hr RCF experiment (a) and the RVF experiment (b).

4. DISCUSSION

4.1 Apparatus Accuracy and Precision

The R1D apparatus produced reproducible BTCs from mixing end-member chemistries. EC appeared to be transported conservatively. The 94.86% and 95.11% total water recoveries for the RCF and RVF experiments, respectively, mean that, although precise, the pump calibration curves were not very accurate. This inaccuracy was likely caused by back-pressure in the R1D apparatus while measuring flow rates during calibrating the pumps. When manual volumetric flux measurements were made a few drops of water continued to flow from the effluent end of the column into the falcon tubes after the pumps were turned off. These additional drops were likely due to draining water from back pressure built up in the probe flow cells and the column from the recent pumping. This would have increased the slope (m) of the calibration curve used for the RCF and RVF experiments, causing a higher predicted flux than was actually occurring under continuously flowing conditions in the RCF and RVF experiments. The solution to this problem is to remove the collection tubes during calibration to avoid collecting drops from releasing back pressure.

4.2 AGW and ASW Breakthrough Curves

The successful logging of the in-line effluent probes demonstrates the R1D can perform data logging in parallel with running the timing of switching between reservoirs and the changing direction and magnitude of the volumetric fluxes in the experiments. Effluent pH dipped to unexpectedly low values (3-4) when DI water (ASW) was being expelled from the column but increased to a more reasonable value of 6 as AGW exited the column. These unusually low pH values suggest a poorly calibrated pH probe. Effluent ORP remained stable at

approximately 319 mV for both experiments, which shows both reservoir waters were oxic, which was expected since the reservoir carboys were covered to prevent dry dust deposition but open to the lab atmosphere, permitting O_2 dissolution.

The progressively lower peak EC values in the BTCs over the course of the RCF and RVF experiments (Figs 7-8) compared to the anticipated 1823 µS/cm GW signal are likely the result the EC probes experiencing a fringe effect in the both the acrylic flow cell and the plastic sampling falcon tube. The fringe effect is where an EC probe interacts with nonconductive container walls, reducing the measured EC of the sample. The inline EC probe was calibrated in a glass beaker rather than installed in the system. Hence, when the probe was reinstalled in the apparatus, EC readings were systematically shifted downwards due to the fringe effect.

For future investigations, in-situ calibration of the probe in the apparatus for EC measurements should be performed for improved accuracy. Probe drift does not seem to be the cause for the progressively downward shift in peak BTC EC values since both the in-line and sample datasets trend downwards at approximately the same rate. It is unlikely for two separate EC probes from different manufacturers to drift at the same rate. Comparison of the 1413 µS/cm standard solution measured with the handheld probe before and after the RCF experiment only found a -1.77% drift. Thus drift in the hand-held probe does not explain the ~10% downward drift in EC measurements observed over the experiment.

Nonconservative behavior of the Na^+ or Cl^- in the tracer is unlikely. Cation exchange capacity (CEC) of quartz is very low (0.6-5.3 cmol/kg) (Hillier, 2003). The medium sand grains used in these experiments have a much lower surface area (4.5 m^2/kg) than silt sized particles (45.4 m^2/kg) (Foth, 1978). This would reduce the surface area available for cation exchange. Moreover, Na^+ exchange is not significant when pH is lower than approximately 8 owing to

positively charged amphoteric Fe-oxide surfaces (Dzombak & Morel, 1990; Rundberg et al., 1994). Anion exchange for chloride with Fe-oxides does not appear to be favorable unless Fe-oxides are substituted for cations with larger positive charges or if pH is lowered resulting in more positive pH surfaces (Borggaard, 1984; Dzombak & Morel, 1990; Tessens & Zauyah, 1982). But, chloride adsorption to Fe-oxides has only been observed in low pH soils and synthetic Fe-oxides (Borggaard, 1984) and does not appear to have been investigated for medium quartz sands. Additionally, our measured low pH values are likely not realistic, rather pH may be closer to neutral. Therefore, low quartz CEC, low affinity for chloride, and low available surface area for any Fe-oxide coatings is not expected to result in significant chloride adsorption and deviation from nonconservative behavior.

Prior to the experiments, the column was well flushed (>20 PV) over the course of several months prior using DI and NaCl. It was noted during an unsuccessful attempted experiment that fine material was flushed from the column, resulting in an unusually high EC signal, which progressively decreased with each NaCl solution flushing event. The manufacturers of the sand report 0.8% of sand particles were less than 149 μm in diameter. It is possible that the repeated flushing of the column was not sufficient to remove all mobilizable fines, and future experiments should consider sediment dispersion and possibly filtration if EC is to be used as a conservative tracer.

Both the RCF and RVF BTCs are identical when plotted against PVs and not time, despite having differing flow regimes. This was expected since the dispersivity of solutes in a porous media depends primarily on distance rather than on time (Bear, 1961). Moreover, since both BTCs and recovered masses are nearly identical, this demonstrates that the R1D apparatus

can execute both simple abrupt constant magnitude flux reversing experiments and more complex variable magnitude flux experiments.

The 1-D numerical model represents a first step towards more advanced reactive flow and transport models. The lack of fit in the RVF experiment to the hydraulic parameters derived from fitting the model to observations of EC in the RCF experiment would appear to reject H1. This apparent dependency of dispersivity on flow velocities, however, can be attributed to a limitation with the modeling software. The Visual MODFLOW software cannot compute head values less than 1 mm at constant head boundary conditions. MODFLOW rounds input head values to the nearest 0.001 m, which is a significant source of error for the variable flow column experiment results. The input head dataset was comprised of 288 values over the entire experiment (72 head steps per 6 hr cycle), but after rounding, only 48 steps (12 steps per cycle) were used in the model (Fig. D2). This rounding artificially coarsened the head used in the MODFLOW model, shifting the model breakthrough curve to the left, when using the same fitting parameters as the constant flux model. Although this suggests a higher advective flux than was present in the RVF experiment (lower porosity), it represents a limitation of the model. This demonstrates that the MODFLOW software is not able to accurately simulate fluxes used in R1D type column experiments. For future investigations, a numerical model should be developed or utilized that uses variable flux boundary conditions.

This rounding in hydraulic heads at the influent boundary did not appear to be a significant source of error for the RCF experiments. The constant heads input into the model were specified to at least three significant figures (0.0558 m and 0.0596 m). Upon rounding to the nearest 0.001 m, the model input heads became 0.056 m and 0.060 m, resulting in a 0.4% and

0.7% percent error, respectively, for the constant flow experiment, which should not impact estimates of n_e and α significantly.

Fluxes within real-world HZs are likely characterized by periods of advection-dominated transport at peak flow and diffusion dominated transport during stagnant flow periods like high tide. The volumetric fluxes are likely not well characterized by simple sine curves since the river stage fluctuation of tidally influenced rivers does not follow this. Furthermore, the river stage pressure pulse propagates into the shallow aquifer which dampens the hydraulic head differences between the aquifer and the river (Shuai et al., 2017a), unlike conditions used here. Analytical solutions to describe complex variable ground water and HZ heads can be used to calculate the appropriate Darcy fluxes as input to the R1D apparatus (Liang & Zhang, 2012). When available, advanced numerical models of 2-D riverbanks can also be used for this purpose. These reveal a complex mixing pattern that includes substantial vertical flow, at least in an isotropic aquifer (Shuai et al., 2017a). The Meghna riverbank aquifer's hydraulic anisotropy will tend to align bi-directional flow in the horizontal plane. Typical values of anisotropy for an alluvial aquifer are 2 to 10 (Freeze & Cherry, 1979; Johnson & Morris, 1962), and range from 335 to 2579 in the region of Araihazar where the Meghna river study site is located (Ahmed, 1994; P S K Knappett et al., 2016; Peter S K Knappett et al., 2012; Nakaya et al., 2011; Kathleen A Radloff, 2010; Ravenscroft et al., 2005). Thus, the R1D apparatus can be tailored to real-world flow regimes to test how advection and diffusion transport affect coupled Fe and As cycling and a number of other important biogeochemical reactions that are important for governing mass fluxes of key elements from the continents to the oceans (Seitzinger et al., 2006; Ward et al., 2017).

4.3 Numerical Modeling Results

Qualitative agreement between the R1D breakthrough curve datasets and the MODFLOW model serves as a theory-based check that experiments were successful. Moreover, the model demonstrates a first step towards reactive flow and transport modeling to predict PNRB formation, breakdown, and As fluxes. Both R1D and MODFLOW model breakthrough curves show the same tracer breakthrough curve behavior, showing this model is a reasonable predictor of R1D conservative transport behavior.

Pore throat clogging does not appear to be occurring in the apparatus. The R1D BTC's of the AGW during 0.8-1.2 and 4.8-5.1 PV and the BTC's of the artificial surface water during 2.7-3.2 and 6.5-7.0 PV are effectively identical between cycles. Since the sediment was well packed and tamped, little sediment consolidation should have occurred. After the experiments were terminated, the columns were unpacked and the packing of the sand was found to be effectively unchanged suggesting no apparent consolidation occurred over the +20 PV flushing during of testing runs would have facilitated packing. The BTC's are effectively identical on both the rising and falling limbs of the AGW and ASW, respectively. Coupled with graphical agreement between the R1D observations and the MODFLOW model, this indicates that sediment consolidation and any related pore throat packing did not occur throughout any point in the conservative tracer experiments. If present, the effect of pore throat clogging and sediment consolidation on dispersivity was too small to be observed in these experiments. Hence, for these experiments it is reasonable to assume that dispersion remained constant.

The RCF fit derived peclet number was 537 and the RVF ranged from 103-579 based on the maxima and minimum advective velocities. Peclet numbers greater than 100 indicate that advection controls solute transport more than diffusion through the column experiments

(Cushman & Tartakovsky, 2016). During stagnation periods that occur in between tides, diffusion control solute transport more than dispersion. To achieve a similar Peclet number to a field site the column length can be shortened, or the Q can be lowered by substituting a thinner ID tubing.

Overall, the conservative tracer tests demonstrate the R1D apparatus in-line probe setup worked and continual pH, ORP, and other parameters can continually be measured throughout the experiments. The conservative MODFLOW model a basic template for modeling concentrations from the bi-directional flow column apparatus. This can lead to reactive flow and transport models to back out rate constants and As fluxes to aquifers and rivers tailored to the transient flow regimes found in real-world sites.

4.4. Broader Applications for the Field of Experimental Hydro-biogeochemistry

The R1D is well suited to understand the hydrogeology and geochemistry of As transport in shallow aquifers in Southeast Asia, specifically along the Meghna River. Over 100 million people worldwide are exposed to As contaminated groundwater greater than the World Health Organization's (WHO) recommended limit of 10 μg/L (Fendorf et al., 2010; WHO, 2001). Approximately 36 million of these people reside in Bangladesh on the Ganges-Brahmaputra-Meghna Delta (GMBD) (Kinniburgh & Smedley, 2001).The origin of geogenic arsenic in these shallow alluvial aquifers is attributed to arsenopyrite, biotite, and possibly chlorite transported into the Bengal Basin from Himalaya mountains (Fendorf et al., 2010; Masuda et al., 2012; Seddique et al., 2011). Arsenic weathered from these mineral then adsorb to Fe-oxides on sediment grains in groundwater (Fendorf et al., 2010). Subsurface solid-phase As concentrations in Meghna riverbank sediments commonly range from 600 to 23,000 mg/kg, providing a clue to

potential sources and sinks of As within the delta (Datta et al., 2009). There is a current need to understandthe hydrological and biogeochemical processes driving As transport to, accumulation within, and mobilization from these aquifer-river interfaces. These processes may be important for understanding As cycling across similar low-lying floodplains and deltas with high concentrations of dissolved As in shallow aquifers throughout South and Southeast Asia (Fendorf et al., 2010; Postma et al., 2007; Wallis et al., 2020).

Hydrologic mixing between oxidized river water and anoxic (reducing) groundwater under fully saturated conditions is thought to drive specific biologically-mediated redox reactions that are responsible for the observed As accumulations in riverbank sediments (Berube et al., 2018; Datta et al., 2009; Jung et al., 2015). This mixing has been hypothesized to result in the formation of a permeable natural reactive barrier (PNRB) of iron oxides (Fe-oxides) within a steep, redox transition zone at the interface between aquifers and rivers (Datta et al., 2009). Dissolved Fe(II) arrives from the anoxic aquifer and mixes with river water which precipitates Fe-oxides. These oxides then sorb dissolved As, which is commonly present as both an oxyanion ($HAs(V)O_4^{2-}$) and a neutrally-charged species ($H_3As(III)O_3^o$) at near-neutral pH under iron-reducing redox states (Radloff et al., 2011; Welch & Stollenwerk, 2003) .

Recent investigations have attributed temporary As accumulation and Fe(II) dissolution in Meghna riverbank sediments to tidally controlled redox cycles (Berube et al., 2018; Jung et al., 2015). Once formed, amorphous Fe-oxides can recrystallize into more stable oxides like goethite and magnetite (Pedersen et al., 2005; Sun, et al. 2016a). These stable oxides can potentially sequester As within their crystal structures during recrystallization, providing a chemical shield to its re-mobilization, should the PRNB be subjected to prolonged reducing conditions at a later time (Datta et al., 2009; Pedersen et al., 2006; Sun, Chillrud, Mailloux, &

Bostick, 2016). On a tidally-influenced river, prolonged reducing conditions may occur during wet seasons when high river discharge dampens the propagation of ocean tides (Berube et al., 2018) and inundate floodplains, thereby stalling groundwater discharge to the river (Larsen et al., 2008; Planer-Friedrich et al., 2012). Lastly, actively accreting riverbanks are progressively buried, subjecting those sediments to anoxic, reducing pore-waters which have been observed to mobilized arsenic (Sø et al., 2018; Stahl et al., 2016; Wallis et al., 2020).

The specific transport and biogeochemical reactions that impact As cycling between solid and aqueous phases across the steep redox gradient between shallow aquifers and tidally fluctuating rivers on the GBMD are not well understood (Fendorf et al., 2010). The chemical reactions are difficult to isolate in the field because of complex 3-D flow patterns that make it challenging to calculate mass balances along a discrete flow paths (Desbarats et al., 2014; Mozumder et al., 2020), as well as physically and chemically heterogeneous sediments. Furthermore, where they exist, PNRBs have been developing since the river first cut through that part of the Holocene sediments (Wilson & Goodbred, 2015), so there is no way to observe their initial formation. For all these reasons, a controlled laboratory experiment is necessary to reproduce the field conditions in a controlled environment to examine hydrological and biogeochemical processes that impact As accumulation and release from riverbanks sediments.

An R1D column experiment can control exact volumetric fluxes of water entering a sand column and measurements of effluent chemistry. This permits determining the spatial distribution of Fe-oxides and bound As and Fe(II) and the types of iron oxides they became sequestered in before and after the experiment(Sun, et al., 2016a; Sun et al., 2016b; Zhang and Selim, 2011). Together, this information, combined with a numerical model, can predict the fate of dissolved Fe(II) and As that enters the sand. Additionally, this approach will help understand

the influence of flow conditions on the chemical reactions that lead to Fe and As accumulation on the solid-phase based on end-member chemical compositions (i.e., aquifer and river) on these. In these riverbanks, the hydrologic and biogeochemical processes are coupled. Understanding the hydro-biogeochemical processes should lead to more accurate quantification of As mass fluxes across Southeast Asian deltas.

Moreover, the flow rate the R1D apparatus can generate are directly applicable to a recent field site along the Meghna River in Bangladesh. The R1D apparatus v calculated via n_e and for the RCF and RVF experiments (0.0251-0.909 m/d) encompass the average linear velocity ranges experienced by the Meghna Riverbanks (0.22-0.4 m/d) (Berube et al., 2018). Sediments from the Meghna Riverbank can be obtained and used as the column matrix with intact microbial communities to facilitate rapid precipitation and reductive dissolution of iron oxides (Berube et al., 2018; Datta et al., 2009). Two artificial reservoirs can be filled with ASW and AGW with similar composition to that in the Meghna River and the shallow alluvial groundwater, respectively. Then, the exact As, Fe, and solute fluxes between the local shallow aquifer and the Meghna River can be estimated since the column contains natural sediment providing the local microbial fauna and mineral phases and the column is subjected to similar flux regimes to those in Bangladesh. The equilibrium, kinetic, and irreversible sorption rate constants for As could then be determined through a joint reactive flow and transport model combined with a multi-reaction model, (Zhang & Selim, 2005).

As well as describing the genesis of a PNRB, the R1D could be utilized to examine the role of DOC on the degradation of a PNRB in these riverbank environments. Oxidation of pore water DOC by microbes reduces Fe(III) to Fe(II), breaking down Fe-oxides in Bangladesh sediments in shallow alluvial aquifers, which can release As into pore waters (Berube et al.,

2018; Datta et al., 2009; Fendorf et al., 2010; McArthur et al., 2001; Nickson et al., 2000).Increasing the amount of available DOC for microorganisms could accelerate PNRB breakdown. In the shallow alluvial aquifers in Bangladesh, DOC is significantly more concentrated in mud deposits (Mihajlov et al., 2020). Moreover, two major sediment types are present in these riverbanks consisting of grey sand, which has little Fe-oxides and higher dissolved Fe(II), As(III), and DOC compared to orange sands (Fendorf et al., 2010; Mozumder et al., 2020). The apparatus reservoirs could be amended with different groundwater and river water DOC mixtures to observe the priming effect on PNRB structure and As liberation.

In addition to Fe-As systems, the R1D apparatus could be applied to explore the interactions between flow rate and reaction kinetics and the supplies of oxidizing and reducing agents to denitrification and nitrification processes in the hyporheic zone. Hyporheic zones are important sources and sinks for nitrogen in aquatic ecosystems (Merill & Tonjes, 2014; Zarnetske et al., 2011). For example, denitrification of nitrate (NO_3^-) in surface water occurs in HZs under the influence of river stage fluctuations. The efficiency of this process is influenced by the period and amplitude of river stage fluctuations (Shuai et al., 2017b). Denitrification of nitrate and nitrification of NH_4^+ in the HZ is controlled by dissolved oxygen (DO), organic carbon availability, microbial communities, initial NO_3^- and NH_4^+ concentrations, and the direction and magnitude of pore-water flux (Liu et al., 2017; Merill & Tonjes, 2014; Sawyer et al., 2009; Shuai et al., 2017b). It is generally found that short residence times favor nitrification, while longer residence times favor denitrification (Merill & Tonjes, 2014; Shuai et al., 2017b; Zarnetske et al., 2011). Lower DO concentrations favor denitrification while higher DO favor nitrification of NH_4^+ (Craig et al., 2010; Merill & Tonjes, 2014).

There do not appear to be many laboratory-based experiments examine the coupled processes of reversing flow regimes in hyporheic zones and biogeochemical factors controlling denitrification. Two manual reversing flux column experiments examined the role of microbial communities on denitrification in the HZ in response to mixing of groundwater and surface waters (Li et al., 2020; Liu et al., 2017). The fully automated R1D setup can simulate the transient flow regimes these HZ experience rather than using abrupt constant flux reversals, which would contribute to understanding the role of advection and diffusion on denitrification. Factorial style experiments could be conducted with a well-known riverbank sediments and intact microorganism communities, such as described in Sawyer et al. (2009) or Liu et al. (2017) along the Colorado River near Austin TX and along the Colombia River at the Hanford site in Washington State. These experiments could examine the synergistic effects of DOC, reversing flux regimes, DO, and influent NO_3^- and NH_4^+ concentrations to understand the mechanisms of how these parameters in tandem control denitrification.

Dissolved organic carbon is important for controlling microbially mediated denitrification and reduction of Fe-oxides which could release As from PNRB's. Denitrification and Fe(III) reduction kinetics increase with the amount of available dissolved organic carbon (DOC) in the HZ (Bardini et al., 2012; Fischer et al., 2005; Han et al., 2019; Merill & Tonjes, 2014; Shuai et al., 2017b) Concentration of DOC is not the most important factor, however. The rate of respiration in HZs is accelerated by the mixing contrasting DOC compositions which are unique to surface water and groundwater (Stegen et al., 2018). This is the so-called priming effect. It is possible that this DOC priming effect and the proportions of favorable and unfavorable DOC can accelerate or deaccelerate denitrification and Fe(III) reduction and As release in the HZ. However, to the best of the author's knowledge, no studies or experiments

have been performed that examine the interaction of the priming effect with bi-directional flow regimes on As, Fe or N cycling in riverbank aquifers.

A set of R1D experiments could investigate the DOC priming effect on denitrification and Fe-oxide reduction. Natural sediments could be collected from known field sites with their corresponding surface and groundwaters and subjected to transient flux regimes in the column analogously to the real world. Coupled with field measurements of the same parameters and numerical modeling, the column experiments could be used to confirm if the DOC priming effect can impact denitrification and Fe-oxide reduction in real-world hyporheic zones.

5. CONCLUSIONS

A novel reversing flux column experiment apparatus has been constructed and is well suited to conduct geochemistry related questions for sediment-water interactions in hyporheic zones. The apparatus can generate accurate and precise flux rates throughout an experiment. It can produce a wide range of volumetric fluxes and range of conditions analogous to real field sites. A numerical model verified that the flux regimes observed in the R1D are realistic and reproducible through groundwater flux and transport theory. This first-of-its-kind apparatus is ready to expand our knowledge of coupled geochemical and hydrological processes in bidirectional flow hyporheic zones. Future work will involve using the R1D to understand the mechanisms of PNRB genesis, breakdown, and As transport along the Meghna River, and the interactions of hydrological and geochemical factors that control denitrification, and the DOC priming effect in the hyporheic zone.

References

Ahmed, K. M. (1994). Hydrogeology of the Dupi Tila aquifer of the Barind tract, NW Bangladesh. *University of London, London*.

ASTM, D., & others. (2011). *Standard practice for classification of soils for engineering purposes (unified soil classification system)*. West Conshohocken, PA.

Bardini, L., Boano, F., Cardenas, M. B., Revelli, R., & Ridolfi, L. (2012). Nutrient cycling in bedform induced hyporheic zones. *Geochimica et Cosmochimica Acta*, *84*, 47–61.

Bear, J. (1961). Some experiments in dispersion. *Journal of Geophysical Research*, *66*(8), 2455–2467.

Berube, M., Jewell, K., Myers, K. D., Knappett, P. S. K., Shuai, P., Hossain, A., Lipsi, M., Hossain, S., Hossain, A., Aitkenhead-Peterson, J., Ahmed, K. M., & Datta, S. (2018). The fate of arsenic in groundwater discharged to the Meghna River, Bangladesh. *Environmental Chemistry*, *15*(1–2), 29–45. https://doi.org/10.1071/EN17104

Bianchin, M. S., Smith, L., & Beckie, R. D. (2011). Defining the hyporheic zone in a large tidally influenced river. *Journal of Hydrology*, *406*(1–2), 16–29.

Bianchin, M., Smith, L., & Beckie, R. (2010). Quantifying hyporheic exchange in a tidal river using temperature time series. *Water Resources Research*, *46*(7).

Boggs Jr, S. (2014). *Principles of sedimentology and stratigraphy*. Pearson Education.

Borggaard, O. K. (1984). Influence of iron oxides on the non-specific anion (chloride) adsorption by soil. *Journal of Soil Science*, *35*(1), 71–78.

Brooks, P. D., & Lemon, M. M. (2007). Spatial variability in dissolved organic matter and inorganic nitrogen concentrations in a semiarid stream, San Pedro River, Arizona. *Journal of Geophysical Research: Biogeosciences*, *112*(G3).

Brush, C. F., Ghiorse, W. C., Anguish, L. J., Parlange, J.-Y., & Grimes, H. G. (1999). *Transport of Cryptosporidium parvum oocysts through saturated columns*.

Butturini, A., Bernal, S., Sabater, S., & Sabater, F. (2002). The influence of riparian-hyporheic zone on the hydrological responses in an intermittent stream. *Hydrology and Earth System Sciences*, *6*(3), 515–526.

Craig, L., Bahr, J. M., & Roden, E. E. (2010). Localized zones of denitrification in a floodplain aquifer in southern Wisconsin, USA. *Hydrogeology Journal*, *18*(8), 1867–1879.

Cushman, J. H., & Tartakovsky, D. M. (2016). *The handbook of groundwater engineering*. CRC Press.

Datta, S., Mailloux, B., Jung, H. B., Hoque, M. A., Stute, M., Ahmed, K. M., & Zheng, Y. (2009). Redox trapping of arsenic during groundwater discharge in sediments from the Meghna riverbank in Bangladesh. *Proceedings of the National Academy of Sciences of the United States of America*, *106*(40), 16930–16935. https://doi.org/10.1073/pnas.0908168106

Desbarats, A. J., Koenig, C. E. M., Pal, T., Mukherjee, P. K., & Beckie, R. D. (2014).

Groundwater flow dynamics and arsenic source characterization in an aquifer system of West Bengal, India. *Water Resources Research*, *50*(6), 4974–5002.

Driscoll, F. G. (1986). *Groundwater and wells 2nd edn*. Johnson Division, St. Paul.

Duff, J. H., & Triska, F. J. (2000). *Nitrogen biogeochemistry and surface-subsurface exchange in streams*.

Dzombak, D. A., & Morel, F. M. M. (1990). *Surface complexation modeling: hydrous ferric oxide*. John Wiley & Sons.

Ellis, B. K., Stanford, J. A., & Ward, J. V. (1998). Microbial assemblages and production in alluvial aquifers of the Flathead River, Montana, USA. *Journal of the North American Benthological Society*, *17*(4), 382–402.

Fendorf, S., Michael, H. A., & Van Geen, A. (2010). Spatial and temporal variations of groundwater arsenic in South and Southeast Asia. *Science*, *328*(5982), 1123–1127. https://doi.org/10.1126/science.1172974

Fetter, C. W., Boving, T. B., & Kreamer, D. K. (1999). *Contaminant hydrogeology* (Vol. 500). Prentice hall Upper Saddle River, NJ.

Fischer, H., Kloep, F., Wilzcek, S., & Pusch, M. T. (2005). A river's liver--microbial processes within the hyporheic zone of a large lowland river. *Biogeochemistry*, *76*(2), 349–371.

Foth, H. D. (1978). *Fundamentals of Soil Science*. Wiley & Sons, Inc.

Freeze, R. A., & Cherry, J. A. (1979). *1979, Groundwater. Englewood Cliffs, NJ: Prentice-Hall*.

Fritz, B. G., & Arntzen, E. V. (2007). Effect of rapidly changing river stage on uranium flux through the hyporheic zone. *Groundwater*, *45*(6), 753–760.

Galler, J. J., & Allison, M. A. (2008). Estuarine controls on fine-grained sediment storage in the Lower Mississippi and Atchafalaya Rivers. *Geological Society of America Bulletin*, *120*(3–4), 386–398.

Gu, C., Hornberger, G. M., Mills, A. L., Herman, J. S., & Flewelling, S. A. (2007). Nitrate reduction in streambed sediments: Effects of flow and biogeochemical kinetics. *Water Resources Research*, *43*(12).

Han, Y.-S., Park, J.-H., Kim, S.-J., Jeong, H. Y., & Ahn, J. S. (2019). Redox transformation of soil minerals and arsenic in arsenic-contaminated soil under cycling redox conditions. *Journal of Hazardous Materials*, *378*, 120745.

Harbaugh, A. W., Banta, E. R., Hill, M. C., & McDonald, M. G. (2000). Modflow-2000, the u. s. geological survey modular ground-water model-user guide to modularization concepts and the ground-water flow process. *Open-File Report. U. S. Geological Survey*, *92*, 134.

Hillier, S. (2003). *Soil Mineralogy with Environmental Applications, edited by JB Dixon and DG Schulze. Soil Science Society of America, Madison, Wisconsin, 2002; xxix+ 866 pages.[ISBN: 0-89118-839-8]. Price $90*. Clay Minerals Society.

Johnson, A. I., & Morris, D. A. (1962). Physical and hydrologic properties of water-bearing

deposits from core holes in the Los Banos-Kettleman City area, California: US Geol. *Survey Open-File Report*.

Jung, H. B., Zheng, Y., Rahman, M. W., Rahman, M. M., & Ahmed, K. M. (2015). Redox zonation and oscillation in the hyporheic zone of the Ganges-Brahmaputra-Meghna Delta: Implications for the fate of groundwater arsenic during discharge. *Applied Geochemistry*, *63*, 647–660. https://doi.org/10.1016/j.apgeochem.2015.09.001

Kinniburgh, D. G., & Smedley, Pl. (2001). *Arsenic contamination of groundwater in Bangladesh*.

Knappett, P S K, Mailloux, B. J., Choudhury, I., Khan, M. R., Michael, H. A., Barua, S., Mondal, D. R., Steckler, M. S., Akhter, S. H., Ahmed, K. M., & others. (2016). Vulnerability of low-arsenic aquifers to municipal pumping in Bangladesh. *Journal of Hydrology*, *539*, 674–686.

Knappett, Peter S K, Emelko, M. B., Zhuang, J., & McKay, L. D. (2008). Transport and retention of a bacteriophage and microspheres in saturated, angular porous media: Effects of ionic strength and grain size. *Water Research*, *42*(16), 4368–4378.

Knappett, Peter S K, McKay, L. D., Layton, A., Williams, D. E., Alam, M. J., Huq, M. R., Mey, J., Feighery, J. E., Culligan, P. J., Mailloux, B. J., & others. (2012). Implications of fecal bacteria input from latrine-polluted ponds for wells in sandy aquifers. *Environmental Science \& Technology*, *46*(3), 1361–1370.

Larsen, F., Pham, N. Q., Dang, N. D., Postma, D., Jessen, S., Pham, V. H., Nguyen, T. B., Trieu, H. D., Tran, L. T., Nguyen, H., & others. (2008). Controlling geological and hydrogeological processes in an arsenic contaminated aquifer on the Red River flood plain, Vietnam. *Applied Geochemistry*, *23*(11), 3099–3115.

Lewis, J., & Sjöstrom, J. (2010). Optimizing the experimental design of soil columns in saturated and unsaturated transport experiments. *Journal of Contaminant Hydrology*, *115*(1–4), 1–13. https://doi.org/10.1016/j.jconhyd.2010.04.001

Li, Y., Zhu, J., Wang, L., Gao, Y., Zhang, W., Zhang, H., & Niu, L. (2020). Grain size tunes microbial community assembly and nitrogen transformation activity under frequent hyporheic exchange: A column experiment. *Water Research*, 116040.

Liang, X., & Zhang, Y.-K. (2012). Analytical solution for drainage and recession from an unconfined aquifer. *Groundwater*, *50*(5), 793–798.

Liu, Y., Liu, C., Nelson, W. C., Shi, L., Xu, F., Liu, Y., Yan, A., Zhong, L., Thompson, C., Fredrickson, J. K., & others. (2017). Effect of water chemistry and hydrodynamics on nitrogen transformation activity and microbial community functional potential in hyporheic zone sediment columns. *Environmental Science \& Technology*, *51*(9), 4877–4886.

Masuda, H., Shinoda, K., Okudaira, T., Takahashi, Y., & Noguchi, N. (2012). Chlorite—source of arsenic groundwater pollution in the Holocene aquifer of Bangladesh. *Geochemical Journal*, *46*(5), 381–391. https://doi.org/10.2343/geochemj.2.0208

McArthur, J. M., Ravenscroft, P., Safiulla, S., & Thirlwall, M. F. (2001). Arsenic in

groundwater: testing pollution mechanisms for sedimentary aquifers in Bangladesh. *Water Resources Research*, *37*(1), 109–117.

McManamay, R. A., Oigbokie, C. O., Kao, S.-C., & Bevelhimer, M. S. (2016). Classification of US hydropower dams by their modes of operation. *River Research and Applications*, *32*(7), 1450–1468.

Merill, L., & Tonjes, D. J. (2014). A review of the hyporheic zone, stream restoration, and means to enhance denitrification. *Critical Reviews in Environmental Science and Technology*, *44*(21), 2337–2379.

Mihajlov, I., Mozumder, M. R. H., Bostick, B. C., Stute, M., Mailloux, B. J., Knappett, P. S. K., Choudhury, I., Ahmed, K. M., Schlosser, P., & van Geen, A. (2020). Arsenic contamination of Bangladesh aquifers exacerbated by clay layers. *Nature Communications*, *11*(1), 1–9.

Mozumder, M. R. H., Bostick, B. C., Selim, M., Islam, M. A., Shoenfelt, E. M., Ellis, T., Mailloux, B. J., Choudhury, I., Ahmed, K. M., & van Geen, A. (2020). Similar retardation of arsenic in gray Holocene and orange Pleistocene sediments: Evidence from field-based column experiments in Bangladesh. *Water Research*, *183*, 116081.

Musial, C. T., Sawyer, A. H., Barnes, R. T., Bray, S., & Knights, D. (2016). Surface water--groundwater exchange dynamics in a tidal freshwater zone. *Hydrological Processes*, *30*(5), 739–750.

Nakaya, S., Natsume, H., Masuda, H., Mitamura, M., Biswas, D. K., & Seddique, A. A. (2011). Effect of groundwater flow on forming arsenic contaminated groundwater in Sonargaon, Bangladesh. *Journal of Hydrology*, *409*(3–4), 724–736.

Nickson, R. T., McArthur, J. M., Ravenscroft, P., Burgess, W. G., & Ahmed, K. M. (2000). Mechanism of arsenic release to groundwater, Bangladesh and West Bengal. *Applied Geochemistry*, *15*(4), 403–413.

Pedersen, H. D., Postma, D., & Jakobsen, R. (2006). Release of arsenic associated with the reduction and transformation of iron oxides. *Geochimica et Cosmochimica Acta*, *70*(16), 4116–4129. https://doi.org/10.1016/j.gca.2006.06.1370

Pedersen, H. D., Postma, D., Jakobsen, R., & Larsen, O. (2005). Fast transformation of iron oxyhydroxides by the catalytic action of aqueous Fe(II). *Geochimica et Cosmochimica Acta*, *69*(16), 3967–3977. https://doi.org/10.1016/j.gca.2005.03.016

Perkins, T. K., & Johnston, Oc. (1963). A review of diffusion and dispersion in porous media. *Society of Petroleum Engineers Journal*, *3*(01), 70–84.

Planer-Friedrich, B., Härtig, C., Lissner, H., Steinborn, J., Süß, E., Hassan, M. Q., Zahid, A., Alam, M., & Merkel, B. (2012). Organic carbon mobilization in a Bangladesh aquifer explained by seasonal monsoon-driven storativity changes. *Applied Geochemistry*, *27*(12), 2324–2334.

Postma, D., Larsen, F., Minh Hue, N. T., Duc, M. T., Viet, P. H., Nhan, P. Q., & Jessen, S. (2007). Arsenic in groundwater of the Red River floodplain, Vietnam: Controlling geochemical processes and reactive transport modeling. *Geochimica et Cosmochimica Acta*,

71(21), 5054–5071. https://doi.org/10.1016/j.gca.2007.08.020

Radloff, K A, Zheng, Y., Michael, H. A., Stute, M., Bostick, B. C., Mihajlov, I., Bounds, M., Huq, M. R., Choudhury, I., Rahman, M. W., & others. (2011). Arsenic migration to deep groundwater in Bangladesh influenced by adsorption and water demand. *Nature Geoscience*, *4*(11), 793–798.

Radloff, Kathleen A. (2010). *Geochemical and hydrologic determinants of arsenic distribution in sedimentary aquifers in Bangladesh*. Columbia University.

Ravenscroft, P., Burgess, W. G., Ahmed, K. M., Burren, M., & Perrin, J. (2005). Arsenic in groundwater of the Bengal Basin, Bangladesh: distribution, field relations, and hydrogeological setting. *Hydrogeology Journal*, *13*(5), 727–751.

Rundberg, R. S., Albinsson, Y., & Vannerberg, K. (1994). Sodium adsorption onto goethite as a function of pH and ionic strength. *Radiochimca Acta*, *66*(Supplement), 333–340.

Sawyer, A. H., Bayani Cardenas, M., Bomar, A., & Mackey, M. (2009). Impact of dam operations on hyporheic exchange in the riparian zone of a regulated river. *Hydrological Processes: An International Journal*, *23*(15), 2129–2137.

Schoeneberger, P. J., Wysocki, D. A., & Benham, E. C. (2012). *Field book for describing and sampling soils* (3.0). Government Printing Office.

Seddique, A. A., Masuda, H., Mitamura, M., Shinoda, K., Yamanaka, T., Nakaya, S., & Ahmed, K. M. (2011). Mineralogy and geochemistry of shallow sediments of Sonargaon, Bangladesh and implications for arsenic dynamics: focusing on the role of organic matter. *Applied Geochemistry*, *26*(4), 587–599.

Seitzinger, S., Harrison, J. A., Böhlke, J. K., Bouwman, A. F., Lowrance, R., Peterson, B., Tobias, C., & Drecht, G. Van. (2006). Denitrification across landscapes and waterscapes: a synthesis. *Ecological Applications*, *16*(6), 2064–2090.

Shuai, P., Cardenas, M. B., Knappett, P. S. K., Bennett, P. C., & Neilson, B. T. (2017a). Denitrification in the banks of fluctuating rivers: The effects of river stage amplitude, sediment hydraulic conductivity and dispersivity, and ambient groundwater flow. *Water Resources Research*, *53*(9), 7951–7967.

Shuai, P., Cardenas, M. B., Knappett, P. S. K., Bennett, P. C., & Neilson, B. T. (2017b). Denitrification in the banks of fluctuating rivers: The effects of river stage amplitude, sediment hydraulic conductivity and dispersivity, and ambient groundwater flow. *Water Resources Research*, *53*(9), 7951–7967. https://doi.org/10.1002/2017WR020610

Sø, H. U., Postma, D., Vi, M. L., Pham, T. K. T., Kazmierczak, J., Dao, V. N., Pi, K., Koch, C. B., Pham, H. V., & Jakobsen, R. (2018). Arsenic in Holocene aquifers of the Red River floodplain, Vietnam: effects of sediment-water interactions, sediment burial age and groundwater residence time. *Geochimica et Cosmochimica Acta*, *225*, 192–209.

Stahl, M. O., Harvey, C. F., van Geen, A., Sun, J., Thi Kim Trang, P., Mai Lan, V., Mai Phuong, T., Hung Viet, P., & Bostick, B. C. (2016). River bank geomorphology controls groundwater arsenic concentrations in aquifers adjacent to the Red River, Hanoi Vietnam.

Water Resources Research, *52*(8), 6321–6334.

Stegen, J. C., Johnson, T., Fredrickson, J. K., Wilkins, M. J., Konopka, A. E., Nelson, W. C., Arntzen, E. V, Chrisler, W. B., Chu, R. K., Fansler, S. J., & others. (2018). Influences of organic carbon speciation on hyporheic corridor biogeochemistry and microbial ecology. *Nature Communications*, *9*(1), 1–11.

Sun, J., Chillrud, S., Mailloux, B., & Bostick, B. (2016). In situ magnetite formation and long-term arsenic immobilization under advective flow conditions. *Environmental Science & Technology*, *50*(18), 10162–10171.

Sun, J., Chillrud, S. N., Mailloux, B. J., Stute, M., Singh, R., Dong, H., Lepre, C. J., & Bostick, B. C. (2016). Enhanced and stabilized arsenic retention in microcosms through the microbial oxidation of ferrous iron by nitrate. *Chemosphere*, *144*, 1106–1115.

Tatham, S. (2021). *puTTY 0.76* (0.76). https://www.chiark.greenend.org.uk/~sgtatham/putty/

Tessens, E., & Zauyah, S. (1982). Positive permanent charge in Oxisols. *Soil Science Society of America Journal*, *46*(5), 1103–1106.

Wallis, I., Prommer, H., Berg, M., Siade, A. J., Sun, J., & Kipfer, R. (2020). The river--groundwater interface as a hotspot for arsenic release. *Nature Geoscience*, 1–8.

Ward, N. D., Bianchi, T. S., Medeiros, P. M., Seidel, M., Richey, J. E., Keil, R. G., & Sawakuchi, H. O. (2017). Where carbon goes when water flows: carbon cycling across the aquatic continuum. *Frontiers in Marine Science*, *4*, 7.

Weight, W. D. (2008). *Hydrogeology Field Manual* (2nd ed.). McGraw Hill.

Welch, A. H., & Stollenwerk, K. G. (2003). *Arsenic in ground water: geochemistry and occurrence*. Springer Science \& Business Media.

Westbrook, S. J., Rayner, J. L., Davis, G. B., Clement, T. P., Bjerg, P. L., & Fisher, S. J. (2005). Interaction between shallow groundwater, saline surface water and contaminant discharge at a seasonally and tidally forced estuarine boundary. *Journal of Hydrology*, *302*(1–4), 255–269.

WHO. (2001). Environmental health criteria 224: arsenic and arsenic compounds. *World Health Organization, Geneva*, 1–108.

Wilson, C. A., & Goodbred, S. L. (2015). Construction and Maintenance of the Ganges-Brahmaputra-Meghna Delta: Linking Process, Morphology, and Stratigraphy. *Annual Review of Marine Science*, *7*(1), 67–88. https://doi.org/10.1146/annurev-marine-010213-135032

Wondzell, S. M., & Swanson, F. J. (1996). Seasonal and storm dynamics of the hyporheic zone of a 4th-order mountain stream. I: Hydrologic processes. *Journal of the North American Benthological Society*, *15*(1), 3–19.

Yuan-Hui, L., & Gregory, S. (1974). Diffusion of ions in sea water and in deep-sea sediments. *Geochimica et Cosmochimica Acta*, *38*(5), 703–714.

Zarnetske, J. P., Haggerty, R., Wondzell, S. M., & Baker, M. A. (2011). Dynamics of nitrate production and removal as a function of residence time in the hyporheic zone. *Journal of Geophysical Research: Biogeosciences*, *116*(G1).

Zhang, H., & Magdi Selim, H. (2011). Second-order modeling of arsenite transport in soils. *Journal of Contaminant Hydrology*, *126*(3–4), 121–129. https://doi.org/10.1016/j.jconhyd.2011.08.002

Zhang, H., & Selim, H. M. (2005). Kinetics of arsenate adsorption- desorption in soils. *Environmental Science \& Technology*, *39*(16), 6101–6108.

APPENDIX A

Figure A1. This is the master wiring diagram for the experiment apparatus. This presents the visual appearance of each component, breadboards used, and connections between different circuit components present in the experimental apparatus as a reference to the physical instrument where they are primarily housed in the circuitry compartment. Note: the physical layout of these components are not the same orientation as in the R1D. This diagram only shows the connections. External control to the pump is triggered via a 5V digital signal to the serial pin 13 of the pump. A circuit is used an operational amplifier to modify the 1.55-2.75V direct analog current (DAC) to 0-3.3V which was inputted to pin 1 of the pump, and this circuit design was obtained from the Arduino website forum (Carrera, 2015). The solenoid valves are diverting valves, which normally divert water between channels A and B. Actuation of the valve with a 12V current will seal channel B, permitting flow between channels A and C. A relay module powered by an external 5V power source controls the 12V current, and this relay is electronically isolated from the rest of the apparatus circuitry to safeguard the electronics in case of a malfunction (Lowe, 2017). Each Solenoid valve circuit is bridged by a flyback diode to dissipate any voltage spikes that occur when the valve actuates. All part images for the probe circuits were obtained from Atlas Scientific, the Arduino Due from the Arduino website forums, and the 8-chanel relay module from OMNIGATHERUM (Drobe011, 2012; Atlas Scientific | Environmental Robotics, 2021; Buruneau, 2016;). Each probe is connected to an SMA or BNC connecter to the breadboard, which is connected to an EZO chip, which converts the probe signal into a value, which is outputted as a TX/RX signal. Each EZO chip and prober are connected to the main circuitry via a EZO in-line voltage isolation chip to prevent signal interference from other probes and the solenoid valves in the apparatus tubing.

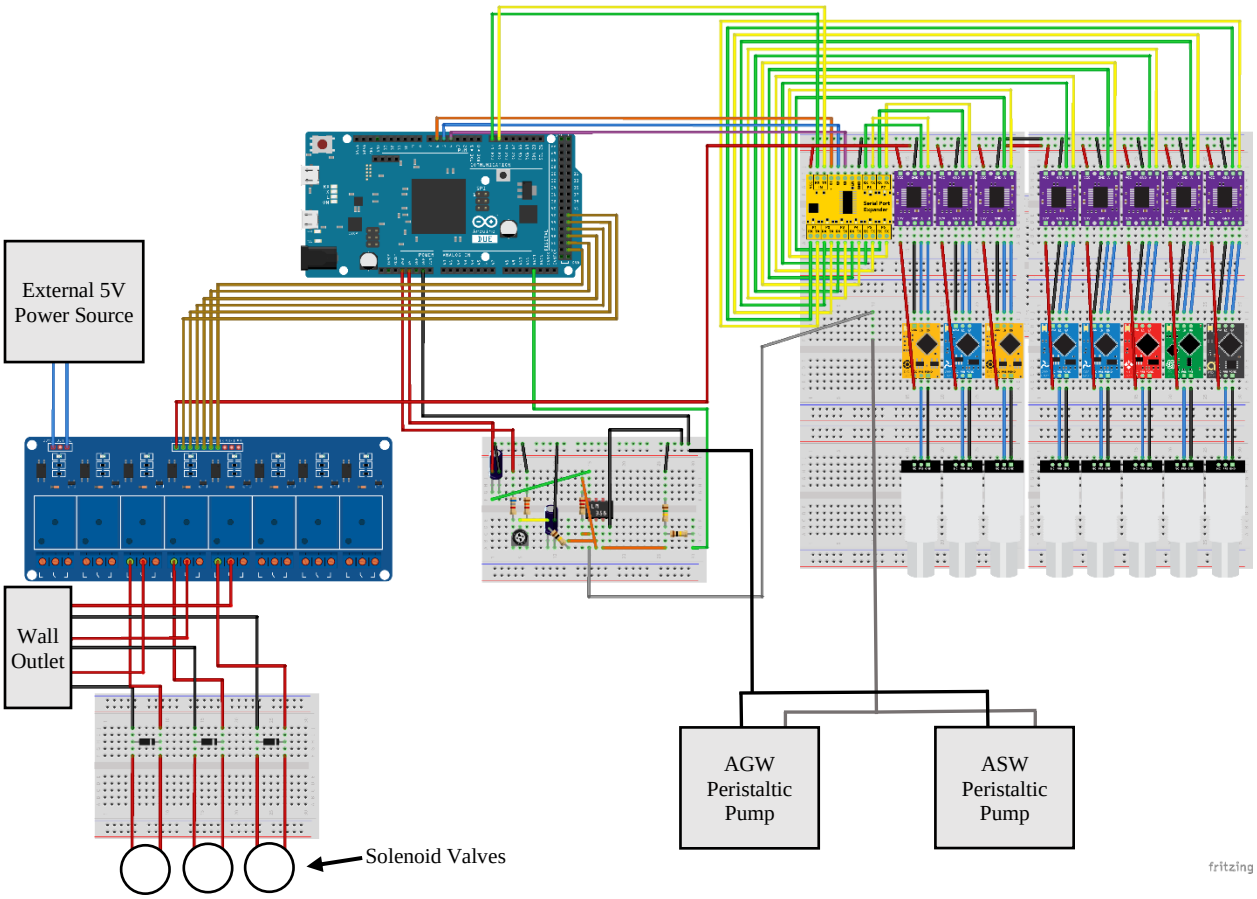

References

Atlas Scientific | Environmental Robotics. (2021). https://atlas-scientific.com/

Carrera, G. (2015). How to modify analog output range of Arduino Due (C) GLP3+. https://create.arduino.cc/projecthub/ArduPic/how-to-modify-analog-output-range-of-arduino-due-6edfb5

Drobe011. (2012). *Arduino Due Fritzing Part*. https://forum.arduino.cc/t/fritzing-part/136458

Lowe, D. (2017). Electronics All-in-one for Dummies. John Wiley \& Sons.

APPENDIX B

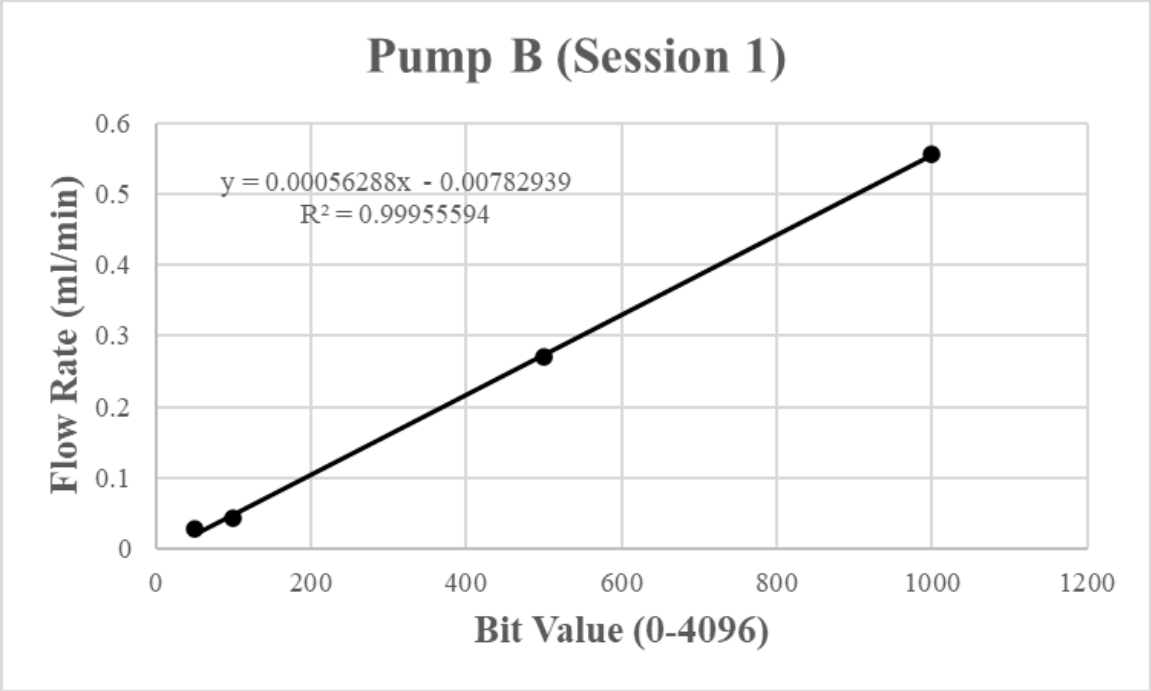

Figure B1. This is the calibration curve for pump B from session #1.

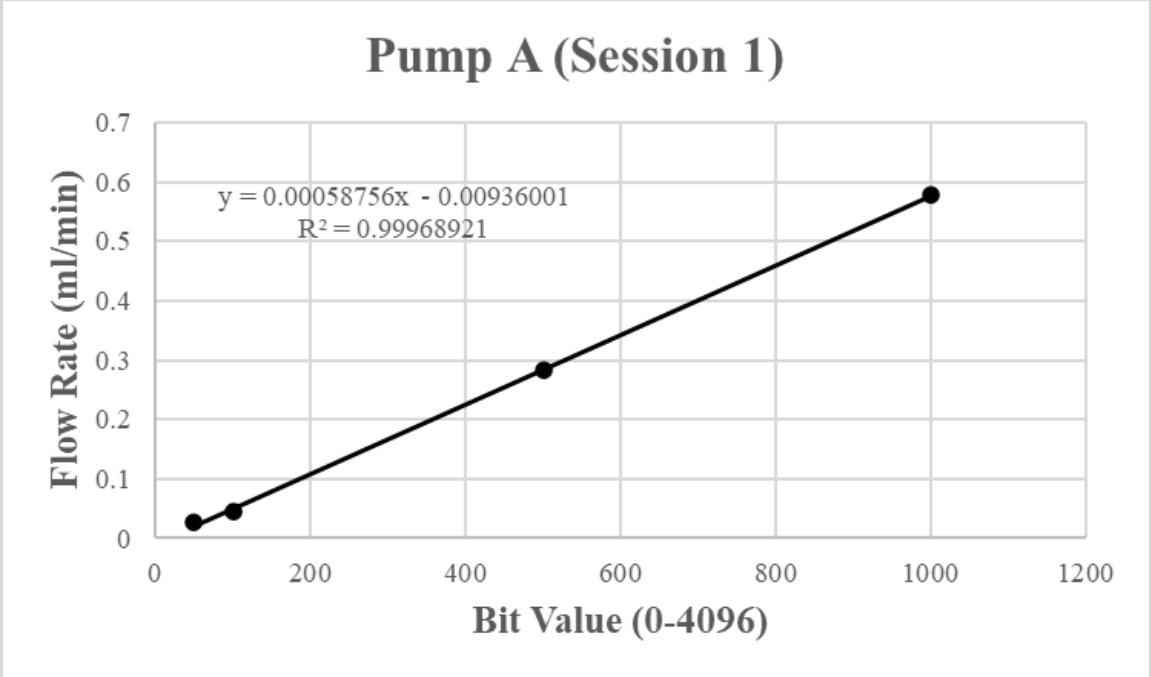

Figure B2. This is the calibration curve for pump A from session #1.

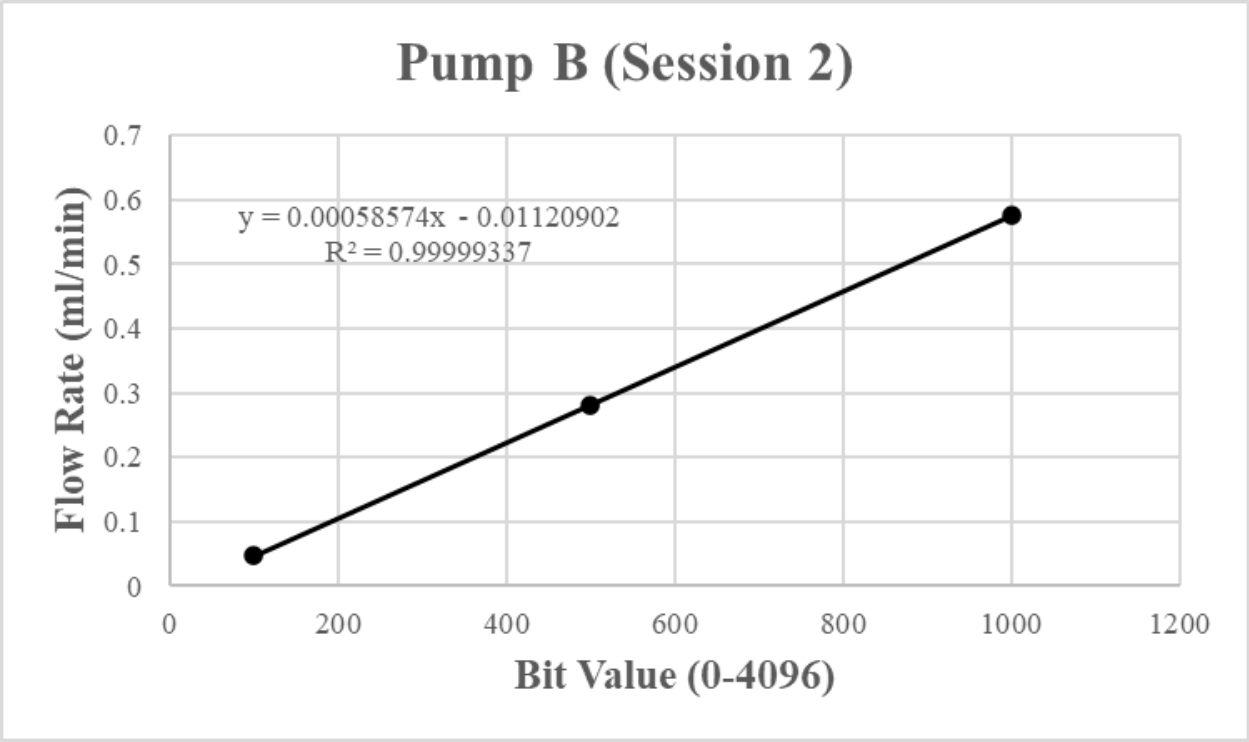

Figure B3. This is the calibration curve for pump B from session #2.

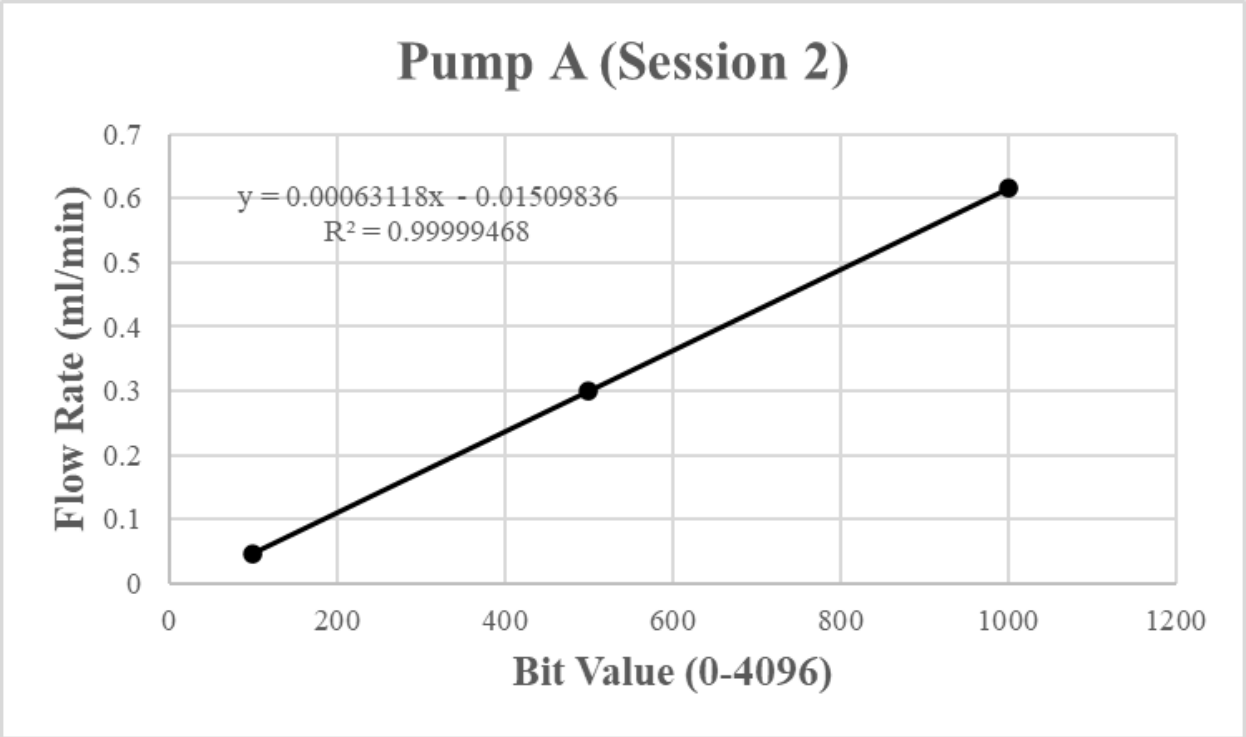

Figure B4. This is the calibration curve for pump A from session #2.

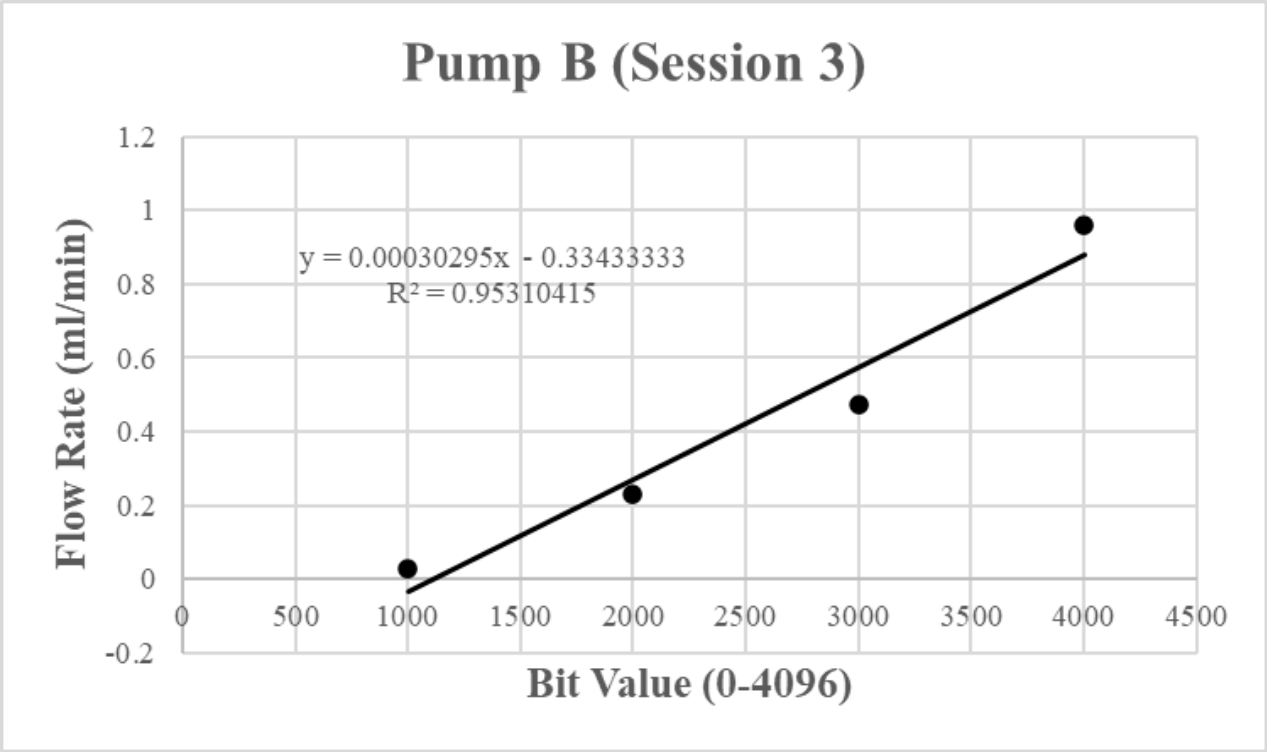

Figure B5. This is the calibration curve for pump B from session #3.

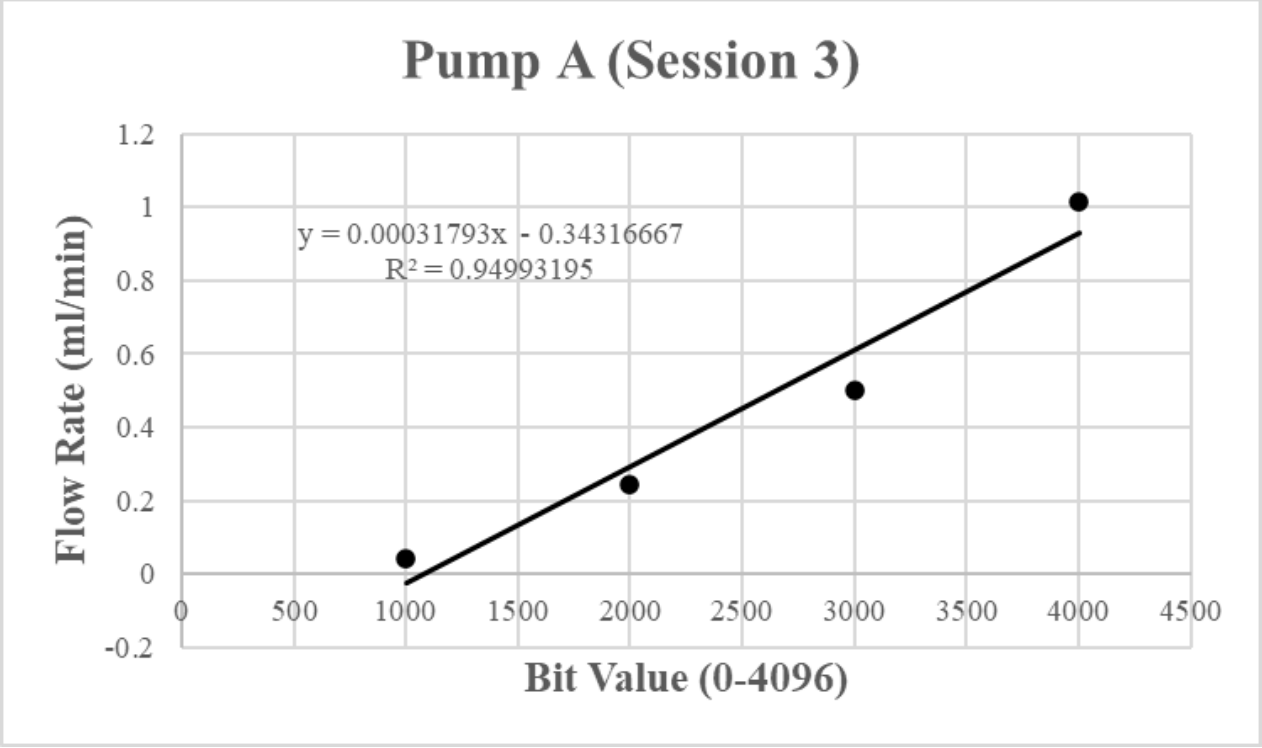

Figure B6. This is the calibration curve for pump A from session #3.

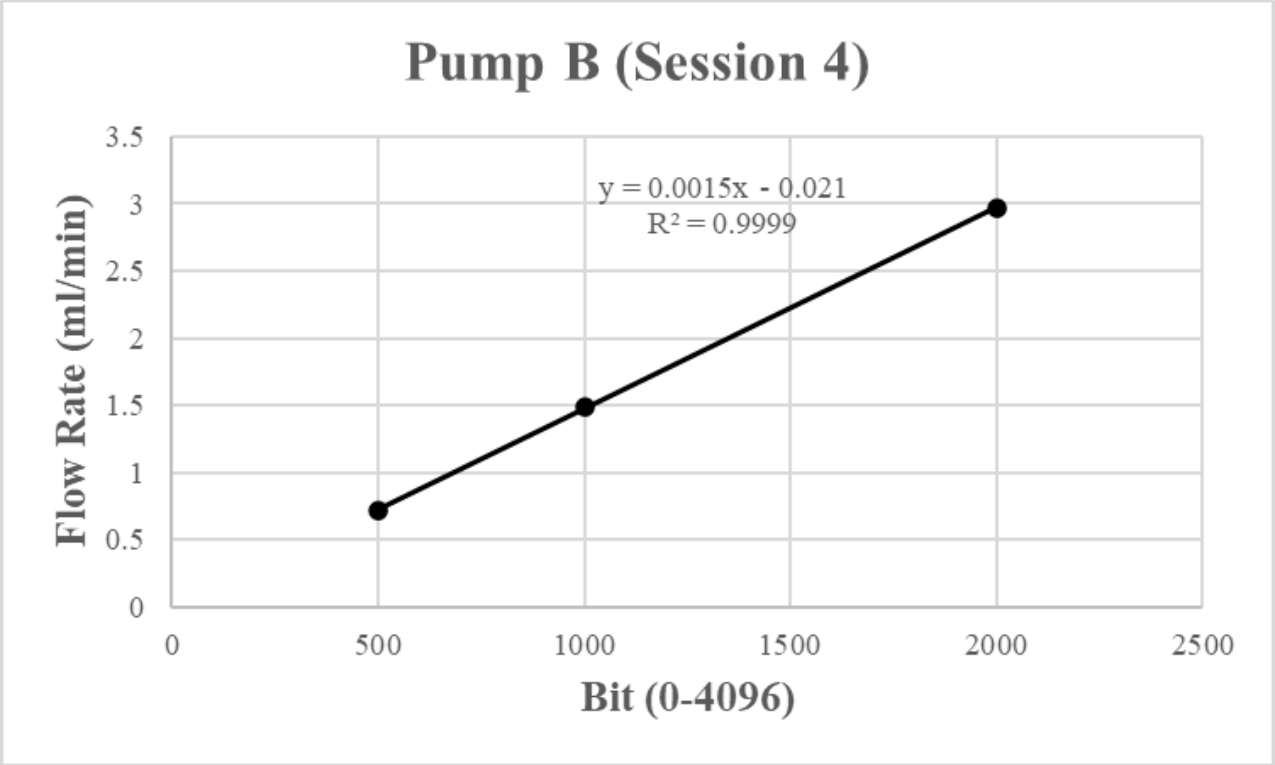

Figure B7. This is the calibration curve for pump B from session #4.

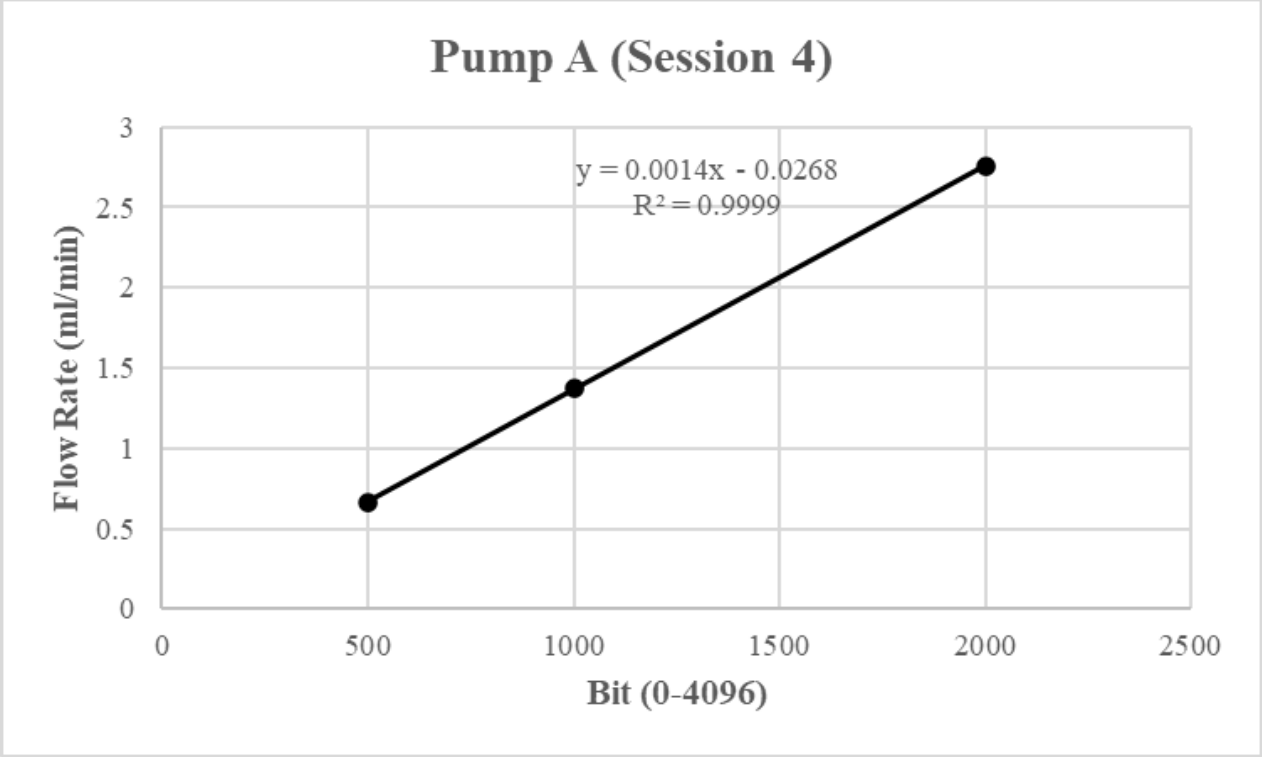

Figure B8. This is the calibration curve for pump A from session #4.

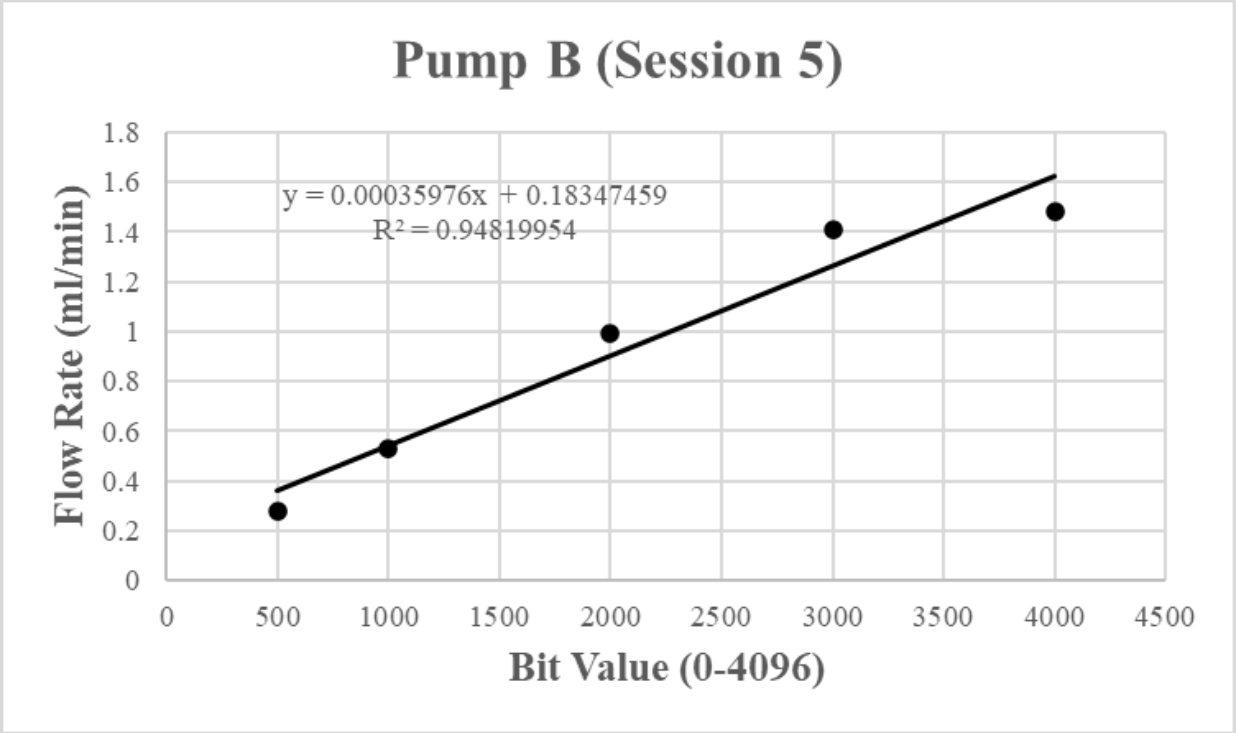

Figure B9. This is the calibration curve for pump B from session #5.

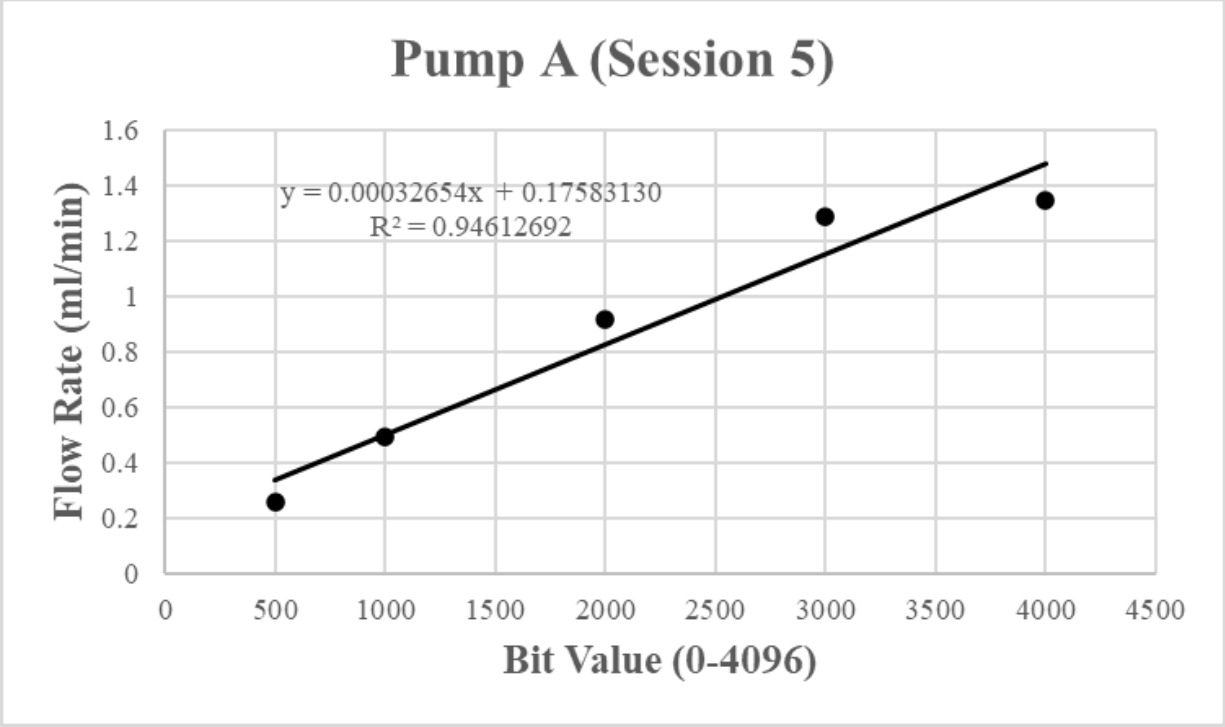

Figure B10. This is the calibration curve for pump A from session #5.

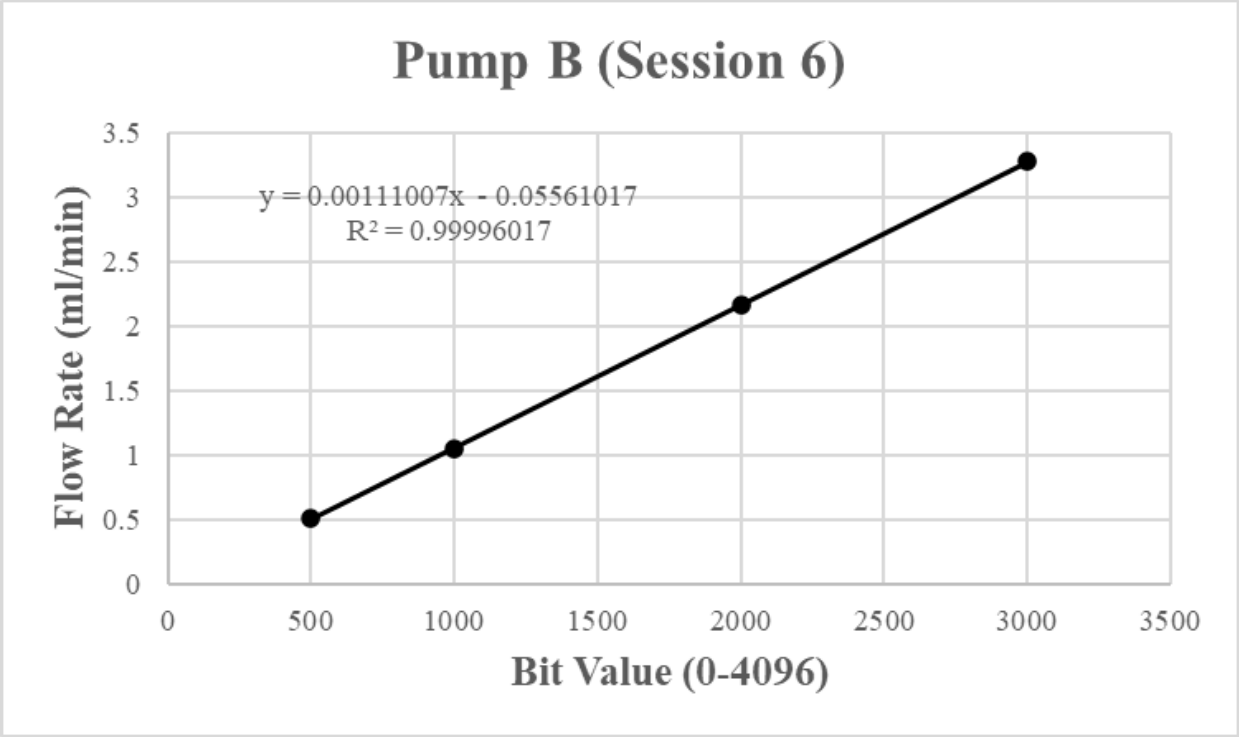

Figure B9. This is the calibration curve for pump B from session #6.

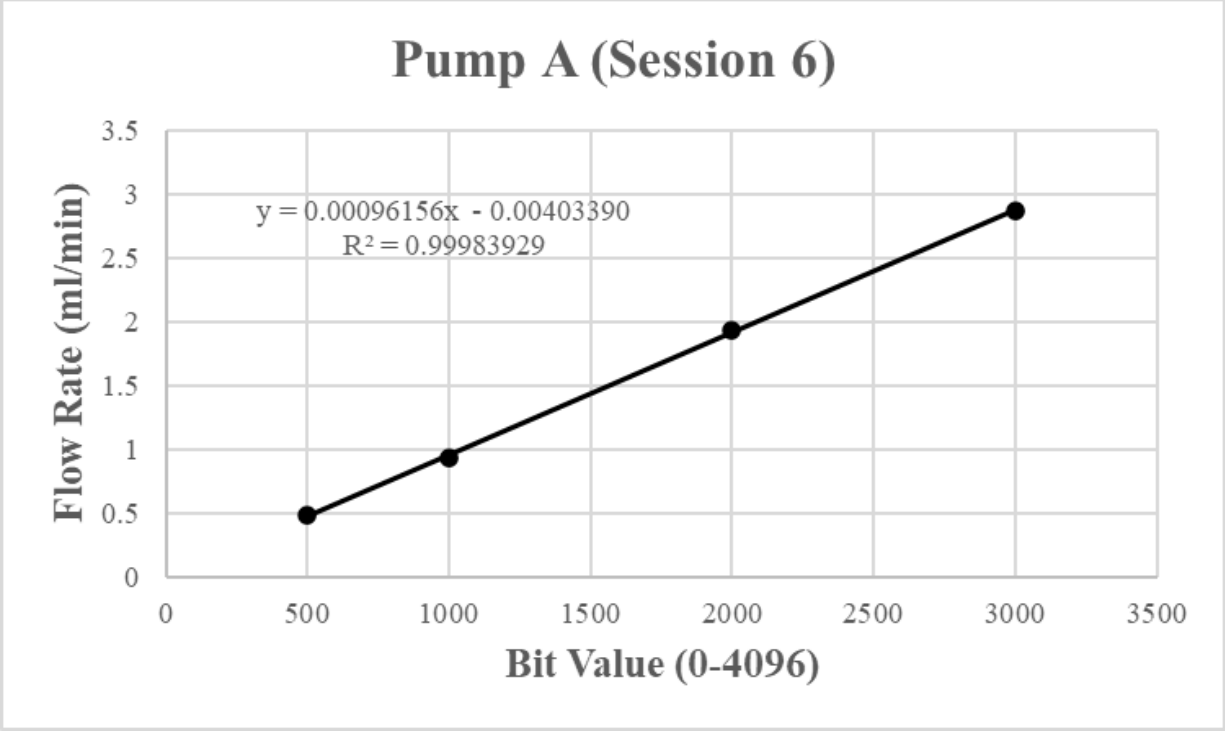

Figure B10. This is the calibration curve for pump A from session #6.

Calibration Session	Pump ID	Output Average Flow Rate (mL/min)							Slope	Intercept	R^2	General Working Flow Range (mL/min)	Tubing ID (mm)
		50 Bits	100 Bits	500 Bits	1000 Bits	2000 Bits	3000 Bits	4000 Bits					
1	B	0.02687±0.00011	0.04290±0.00033	0.2712±0.0013	0.5565±0.0009		-	-	0.000563	-0.00783	0.9996	0.03-1.5	1.00
1	A	0.02573±0.00083	0.04438±0.00019	0.2826±0.0007	0.5793±0.0010		-	-	0.000588	-0.00936	0.9997		1.00
2	B	-	0.04780	0.2809±0.0001	0.5749±0.0001		-	-	0.000586	-0.01121	0.9999	0.03-1.5	1.00
2	A	-	0.04760	0.3013±0.0003	0.6158±0.0006		-	-	0.000631	-0.0151	0.9999		1.00
3	B	-			0.0295±0.0024	0.2317±0.0058	0.4717±0.0198	0.9593±0.0467	0.0003	-0.33433	0.9531	0.0015-0.5	0.79
3	A	-			0.0442±0.0028	0.2422±0.0051	0.5035±0.0009	1.017±0.0126	0.00032	-0.34317	0.9499		0.79
4	B	-	-	0.7168	1.489	2.965	-	-	0.00150	-0.02100		0.05-3	1.59
4	A	-	-	0.6638	1.377	2.758	-	-	0.00139	-0.02680		0.05-3	1.59
5	B	-		0.2790±0.0042	0.5310±0.0063	0.9938±0.0110	1.411±0.011	1.479±0.041	0.0003	0.183475	0.9482	0.03-1.5	1.00
5	A	-		0.2588±0.0093	0.4933±0.0168	0.9153±0.0301	1.291±0.046	1.350±0.060	0.000327	0.175831	0.9462		1.00
6	B	-	-	0.5160±0.0067	1.048±0.0032	2.165±0.0096	3.277±0.0134		0.001107	-0.04725	0.9999	0.05-3	1.59
6	A	-	-	0.4600±0.021	0.9400±0.009	1.919±0.011	2.860±0.014		0.000962	-0.01830	0.9999		1.59

Table 1. This is a table of average flow rates generated per bit value from five pump calibration sessions from Fall 2020-Summer 2021. Each column corresponds to flow rates from each bit value with 95% confidence interval error bars. The slope, intercept, and R2 values are provided. Rough estimates of general working flow range are provided with tubing inner diameters.

Figure B11. This is the final version of the R1D Program Arduino Code. The original codes were modified and significantly expanded from from the commands provided by Atlas Scientific for the 8:1 Serial Port Expander Arduino Mega, EZO DO, EZO ORP, EZO EC, EZO Temperature, and EZO EC circuits.

```
#include <RBD_Timer.h>
long TimeStep = 30*1000; //30s in miliseconds
long CycleInterval = 86400*1000; //one day for this timer to expire
long ExperiimentSInterval = 30*86400*1000UL;//thirty day interval for the experiment timer to expire.
RBD::Timer LoopTimer(TimeStep);
RBD::Timer CycleTimer(CycleInterval);
RBD::Timer ExperimentTimer(ExperiimentSInterval);

//Defining the pins for the apparatus
#define Val_1 47
#define Val_2 49
#define Val_3 51
#define PumpA 43
#define PumpB 45
#define AnalogPumpSwap 53
#define PumpMagnitude DAC0
//4:r<CR>
//To open a channel and not send a command just send the channel number followed by a colon.
//1:<CR>
//3:<CR>
String inputstring = "";                    //a string to hold incoming data from the PC
String sensorstring = "";                   //a string to hold the data from the Atlas Scientific product
boolean input_string_complete = false;      //have we received all the data from the PC
boolean sensor_string_complete = false;     //have we received all the data from the Atlas Scientific product
String TempCompSTR="";
String TempCompReturn="";

//Stuff for collecting data from probes
int s1 = 6;                                 //Arduino pin 6 to control pin S1
int s2 = 5;                                 //Arduino pin 5 to control pin S2
int s3 = 4;                                 //Arduino pin 4 to control pin S3
int Counter = 0;
int MAX=6;
int port = 0;
String portstring="";
String DOprobestring="";
int PortNum = 5;

//**********Initial Variables
```

```
//Slope and intercept are obtained from pump calibrations
double B_Slope = 0.001107028;
double B_Intercept = -0.047254237;
double A_Slope = 0.000961774;
double A_Intercept = -0.018299435;
double MaxFlow = 2.013;//This is the amplitude of the sine wave in ml/min
double Porosity = 0.37;//Sediment porosity via bulk density
double ColumnLength = 20;//column length in cm
double ColumnRadius = 3.15;//Column radius in cm
double NUMCycles = 14; //This states the number of 12 hr cycles containing two eipsodes of 6hr
flow from each reservoir (1 each).

//Calculated Variables
double PoreVolume = sq(ColumnRadius)*3.14159*ColumnLength*Porosity;//This is the
volume of column pores: Column volume*porosity
double CycleCumPoreVolume = 0; //Cumlative pore volumes for each 6hr cycle
double TotalCumPoreVolume = 0; //Cumulative pore volume for the entire experiment
double TotalVolume = 0; //Total volume of water injected for the experiment

void setup() {
  // put your setup code here, to run once:
  pinMode(Val_1,OUTPUT);
  pinMode(Val_2,OUTPUT);
  pinMode(Val_3,OUTPUT);
  pinMode(PumpA,OUTPUT);
  pinMode(PumpB,OUTPUT);
  pinMode(AnalogPumpSwap,OUTPUT);
  digitalWrite(Val_1,HIGH);
  digitalWrite(Val_2,HIGH);
  digitalWrite(Val_3,HIGH);
  digitalWrite(PumpA,HIGH);
  digitalWrite(PumpB,HIGH);
  digitalWrite(AnalogPumpSwap,HIGH);
  Serial.begin(9600);                    //Set the hardware serial port to 9600
  Serial3.begin(9600);                    //set baud rate for software serial port_3 to 9600
  inputstring.reserve(10);                //set aside some bytes for receiving data from the PC
  sensorstring.reserve(30);               //set aside some bytes for receiving data from Atlas
Scientific product
  pinMode(s1, OUTPUT);                        //Set the digital pin as output
  pinMode(s2, OUTPUT);                        //Set the digital pin as output
  pinMode(s3, OUTPUT);                        //Set the digital pin as output
  Serial.println();
  analogWriteResolution(12);

}
```

```
void loop() {
  delay(300000);
  ExperimentTimer.restart();//Start the timer to keep track of time for the entire experiment.

Serial.println("*WA,Temp,A,*SL,*WA,EC,B,*SL,*WA,pH,C,*SL,*WA,ORP_EF,D,*SL,*WA,
ORP_SW,E,*SL,*WA,DO_SW,F,*SL,*WA,ORP_GW,G,*SL,*WA,DO_GW,H,*SL,Volume,P
V_Step,PV_Cycle,PV_Total,TotalTime,CycleTime,LoopTimer,CycleNumber,CycleStep");
    for(int n = 1; n<=NUMCycles; n++){
    // put your main code here, to run repeatedly:
    digitalWrite(Val_1,HIGH);
    digitalWrite(Val_2,HIGH);
    digitalWrite(Val_3,HIGH);
    digitalWrite(PumpB,LOW);
    CycleTimer.restart();//Starts the timer for the 6hr cycle
    for(int i = 1;i<=720;i++){ //This tells the arduino to wait for 24sec and take a reading (6sec
each) resulting in a complete probe set reading to the serial monitor every 30sec. This will loop
for a full 12 hrs
          LoopTimer.restart();
          if ((MaxFlow*sin(i*3.14159/720)-B_Intercept)/B_Slope<60){
          analogWrite(DAC0,0);//This keeps the pumps from reciving a signal below 50bits which
damages them.
          }
          if ((MaxFlow*sin(i*3.14159/720)-B_Intercept)/B_Slope>=60){
          analogWrite(DAC0,floor((MaxFlow*sin(i*3.14159/720)-B_Intercept)/B_Slope));//If the
imput bit is >50, then continue on with the rest of the loop.
          }

          digitalWrite(s1, bitRead(0, 0));          //Here we have two commands combined into
one.
          digitalWrite(s2, bitRead(0, 1));          //The digitalWrite command sets a pin to 1/0
(high or low)
          digitalWrite(s3, bitRead(0, 2));          //The bitRead command tells us what the bit
value is for a specific bit location of a number
          delay(20);                                //this is needed to make sure the channel switching
event has completed
          Serial3.print("R\r");                     //Poll the port for a value
          sensorstring = Serial3.readStringUntil(13);       //read the string until we see a <CR>
          Serial.print(sensorstring);
          Serial.print(",");                        //Poll the port for a value
          Serial3.print("R\r");                     //Poll the port for a value
          sensorstring = Serial3.readStringUntil(13);       //read the string until we see a <CR>
          Serial.print(sensorstring);
          Serial.print(",A,");
          Serial3.print("sleep\r");
          sensorstring = Serial3.readStringUntil(13);       //read the string until we see a <CR>
          Serial.print(sensorstring);
```

```
        Serial.print(",");

        digitalWrite(s1, bitRead(1, 0));            //Here we have two commands combined into
one.
        digitalWrite(s2, bitRead(1, 1));            //The digitalWrite command sets a pin to 1/0
(high or low)
        digitalWrite(s3, bitRead(1, 2));            //The bitRead command tells us what the bit
value is for a specific bit location of a number
        delay(20);                                  //this is needed to make sure the channel switching
event has completed
        Serial3.print("R\r");                       //Poll the port for a value
        sensorstring = Serial3.readStringUntil(13);       //read the string until we see a <CR>
        Serial.print(sensorstring);
        Serial.print(",");                          //Poll the port for a value
        Serial3.print("R\r");                       //Poll the port for a value
        sensorstring = Serial3.readStringUntil(13);       //read the string until we see a <CR>
        Serial.print(sensorstring);
        Serial.print(",B,");
        Serial3.print("sleep\r");
        sensorstring = Serial3.readStringUntil(13);       //read the string until we see a <CR>
        Serial.print(sensorstring);
        Serial.print(",");

        digitalWrite(s1, bitRead(2, 0));            //Here we have two commands combined into
one.
        digitalWrite(s2, bitRead(2, 1));            //The digitalWrite command sets a pin to 1/0
(high or low)
        digitalWrite(s3, bitRead(2, 2));            //The bitRead command tells us what the bit
value is for a specific bit location of a number
        delay(20);                                  //this is needed to make sure the channel switching
event has completed
        Serial3.print("R\r");                       //Poll the port for a value
        sensorstring = Serial3.readStringUntil(13);       //read the string until we see a <CR>
        Serial.print(sensorstring);
        Serial.print(",");                          //Poll the port for a value
        Serial3.print("R\r");                       //Poll the port for a value
        sensorstring = Serial3.readStringUntil(13);       //read the string until we see a <CR>
        Serial.print(sensorstring);
        Serial.print(",C,");
        Serial3.print("sleep\r");
        sensorstring = Serial3.readStringUntil(13);       //read the string until we see a <CR>
        Serial.print(sensorstring);
        Serial.print(",");

        digitalWrite(s1, bitRead(3, 0));            //Here we have two commands combined into
one.
```

```
        digitalWrite(s2, bitRead(3, 1));            //The digitalWrite command sets a pin to 1/0
(high or low)
        digitalWrite(s3, bitRead(3, 2));            //The bitRead command tells us what the bit
value is for a specific bit location of a number
        delay(20);                                  //this is needed to make sure the channel switching
event has completed
        Serial3.print("R\r");                       //Poll the port for a value
        sensorstring = Serial3.readStringUntil(13);       //read the string until we see a <CR>
        Serial.print(sensorstring);
        Serial.print(",");                          //Poll the port for a value
        Serial3.print("R\r");                       //Poll the port for a value
        sensorstring = Serial3.readStringUntil(13);       //read the string until we see a <CR>
        Serial.print(sensorstring);
        Serial.print(",D,");
        Serial3.print("sleep\r");
        sensorstring = Serial3.readStringUntil(13);       //read the string until we see a <CR>
        Serial.print(sensorstring);
        Serial.print(",");

        digitalWrite(s1, bitRead(4, 0));            //Here we have two commands combined into
one.
        digitalWrite(s2, bitRead(4, 1));            //The digitalWrite command sets a pin to 1/0
(high or low)
        digitalWrite(s3, bitRead(4, 2));            //The bitRead command tells us what the bit
value is for a specific bit location of a number
        delay(20);                                  //this is needed to make sure the channel switching
event has completed
        Serial3.print("R\r");                       //Poll the port for a value
        sensorstring = Serial3.readStringUntil(13);       //read the string until we see a <CR>
        Serial.print(sensorstring);
        Serial.print(",");                          //Poll the port for a value
        Serial3.print("R\r");                       //Poll the port for a value
        sensorstring = Serial3.readStringUntil(13);       //read the string until we see a <CR>
        Serial.print(sensorstring);
        Serial.print(",E,");
        Serial3.print("sleep\r");
        sensorstring = Serial3.readStringUntil(13);       //read the string until we see a <CR>
        Serial.print(sensorstring);
        Serial.print(",");

        digitalWrite(s1, bitRead(5, 0));            //Here we have two commands combined into
one.
        digitalWrite(s2, bitRead(5, 1));            //The digitalWrite command sets a pin to 1/0
(high or low)
        digitalWrite(s3, bitRead(5, 2));            //The bitRead command tells us what the bit
value is for a specific bit location of a number
```

```
        delay(20);                          //this is needed to make sure the channel switching
event has completed
        Serial3.print("R\r");                //Poll the port for a value
        sensorstring = Serial3.readStringUntil(13);     //read the string until we see a <CR>
        Serial.print(sensorstring);
        Serial.print(",");                  //Poll the port for a value
        Serial3.print("R\r");                //Poll the port for a value
        sensorstring = Serial3.readStringUntil(13);     //read the string until we see a <CR>
        Serial.print(sensorstring);
        Serial.print(",F,");
        Serial3.print("sleep\r");
        sensorstring = Serial3.readStringUntil(13);     //read the string until we see a <CR>
        Serial.print(sensorstring);
        Serial.print(",");

        digitalWrite(s1, bitRead(6, 0));        //Here we have two commands combined into
one.
        digitalWrite(s2, bitRead(6, 1));        //The digitalWrite command sets a pin to 1/0
(high or low)
        digitalWrite(s3, bitRead(6, 2));        //The bitRead command tells us what the bit
value is for a specific bit location of a number
        delay(20);                          //this is needed to make sure the channel switching
event has completed
        Serial3.print("R\r");                //Poll the port for a value
        sensorstring = Serial3.readStringUntil(13);     //read the string until we see a <CR>
        Serial.print(sensorstring);
        Serial.print(",");                  //Poll the port for a value
        Serial3.print("R\r");                //Poll the port for a value
        sensorstring = Serial3.readStringUntil(13);     //read the string until we see a <CR>
        Serial.print(sensorstring);
        Serial.print(",G,");
        Serial3.print("sleep\r");
        sensorstring = Serial3.readStringUntil(13);     //read the string until we see a <CR>
        Serial.print(sensorstring);
        Serial.print(",");

        digitalWrite(s1, bitRead(7, 0));        //Here we have two commands combined into
one.
        digitalWrite(s2, bitRead(7, 1));        //The digitalWrite command sets a pin to 1/0
(high or low)
        digitalWrite(s3, bitRead(7, 2));        //The bitRead command tells us what the bit
value is for a specific bit location of a number
        delay(20);                          //this is needed to make sure the channel switching
event has completed
        Serial3.print("R\r");                //Poll the port for a value
        sensorstring = Serial3.readStringUntil(13);     //read the string until we see a <CR>
```

```
        Serial.print(sensorstring);
        Serial.print(",");                      //Poll the port for a value
        Serial3.print("R\r");                        //Poll the port for a value
        sensorstring = Serial3.readStringUntil(13);         //read the string until we see a <CR>
        Serial.print(sensorstring);
        Serial.print(",H,");
        Serial3.print("sleep\r");
        sensorstring = Serial3.readStringUntil(13);         //read the string until we see a <CR>
        Serial.print(sensorstring);
        Serial.print(",");

        //Printin out useful stuff here
        Serial.print(float(MaxFlow*sin(i*3.14159/720)),8); //This prints the flow rate during the
step
        Serial.print(",");
        Serial.print(float(MaxFlow*sin(i*3.14159/720)*0.5),8); //This prints the volume
outputted during the step
        Serial.print(",");
        Serial.print(float(MaxFlow*sin(i*3.14159/720)*0.5/PoreVolume),8);//This prints the
pore volume injected during this timestep
        Serial.print(",");
        CycleCumPoreVolume +=MaxFlow*sin(i*3.14159/720)*0.5/PoreVolume;//Adds the
new pore volume to the total pore volume in the cycle
        TotalCumPoreVolume +=MaxFlow*sin(i*3.14159/720)*0.5/PoreVolume;//Adds the new
pore volume to the total pore volume in the experiment
        TotalVolume += MaxFlow*sin(i*3.14159/720)*0.5;//Adds the new water volume to total
volume in the cycle.
        Serial.print(float(CycleCumPoreVolume),8); //This prints the total pore volume for the
experiment's cycle
        Serial.print(",");
        Serial.print(float(TotalCumPoreVolume),8);//This prints the total pore volume injected
during over the entire experiment
        Serial.print(",");
        Serial.print(float(ExperimentTimer.getValue()/1000),8); //Gets the total timestamp for all
looped measurements in seconds
        Serial.print(",");
        Serial.print(float(CycleTimer.getValue()/1000),8); //Gets the total timestamp for this 6hr
cycle in seconds
        Serial.print(",");
        Serial.print(float(LoopTimer.getValue()/1000),8); //Snags the time passed during the loop
after measuring the probes in seconds
        Serial.print(",");
        Serial.print(n); //This prints the number for the 12 hr cycle that the experiment is
currently on. For example; 2 = second of the 12hr cycles.
        Serial.print(",");
```

```
        Serial.print(i); //This prints the 30second timestamp value the column is currently on. For example, 59 = the fifty-nith step.
        Serial.print(",");
        Serial.println(floor((MaxFlow*sin(i*3.14159/720)+B_Intercept)/B_Slope));//This prints out the bit sent to the pump

        while(LoopTimer.getValue()<=LoopTimer.getTimeout()){}
          LoopTimer.stop(); //Stops the loop after exactly 30 second.
          }
   CycleTimer.stop(); //kills the 6hr loop timer
   analogWrite(DAC0,0);
   CycleCumPoreVolume=0;//Wipes the cycle pore volume for the next cycle
   digitalWrite(PumpB,HIGH);//Turns off the pump

   // put your main code here, to run repeatedly:
   digitalWrite(Val_1,LOW);
   digitalWrite(Val_2,LOW);
   digitalWrite(Val_3,LOW);
   digitalWrite(PumpA,LOW);
   CycleTimer.restart();//Starts the timer for the 6hr cycle
   for(int i = 1;i<=720;i++){ //This tells the arduino to wait for 24sec and take a reading (6sec each) resulting in a complete probe set reading to the serial monitor every 30sec. This will loop for a full 12 hrs
        LoopTimer.restart();
        if ((MaxFlow*sin(i*3.14159/720)-A_Intercept)/A_Slope<60){
        analogWrite(DAC0,0);//This keeps the pumps from reciving a signal below 50bits which damages them.
        }
        if ((MaxFlow*sin(i*3.14159/720)-A_Intercept)/A_Slope>=60){
        analogWrite(DAC0,floor((MaxFlow*sin(i*3.14159/720)-A_Intercept)/A_Slope));//If the imput bit is >50, then continue on with the rest of the loop.
        }

        digitalWrite(s1, bitRead(0, 0));          //Here we have two commands combined into one.
        digitalWrite(s2, bitRead(0, 1));          //The digitalWrite command sets a pin to 1/0 (high or low)
        digitalWrite(s3, bitRead(0, 2));          //The bitRead command tells us what the bit value is for a specific bit location of a number
        delay(20);                                //this is needed to make sure the channel switching event has completed
        Serial3.print("R\r");                     //Poll the port for a value
        sensorstring = Serial3.readStringUntil(13);       //read the string until we see a <CR>
        Serial.print(sensorstring);
        Serial.print(",");                        //Poll the port for a value
        Serial3.print("R\r");                     //Poll the port for a value
```

```
        sensorstring = Serial3.readStringUntil(13);        //read the string until we see a <CR>
        Serial.print(sensorstring);
        Serial.print(",A,");
        Serial3.print("sleep\r");
        sensorstring = Serial3.readStringUntil(13);        //read the string until we see a <CR>
        Serial.print(sensorstring);
        Serial.print(",");

        digitalWrite(s1, bitRead(1, 0));            //Here we have two commands combined into
one.
        digitalWrite(s2, bitRead(1, 1));            //The digitalWrite command sets a pin to 1/0
(high or low)
        digitalWrite(s3, bitRead(1, 2));            //The bitRead command tells us what the bit
value is for a specific bit location of a number
        delay(20);                                  //this is needed to make sure the channel switching
event has completed
        Serial3.print("R\r");                       //Poll the port for a value
        sensorstring = Serial3.readStringUntil(13);        //read the string until we see a <CR>
        Serial.print(sensorstring);
        Serial.print(",");                          //Poll the port for a value
        Serial3.print("R\r");                       //Poll the port for a value
        sensorstring = Serial3.readStringUntil(13);        //read the string until we see a <CR>
        Serial.print(sensorstring);
        Serial.print(",B,");
        Serial3.print("sleep\r");
        sensorstring = Serial3.readStringUntil(13);        //read the string until we see a <CR>
        Serial.print(sensorstring);
        Serial.print(",");

        digitalWrite(s1, bitRead(2, 0));            //Here we have two commands combined into
one.
        digitalWrite(s2, bitRead(2, 1));            //The digitalWrite command sets a pin to 1/0
(high or low)
        digitalWrite(s3, bitRead(2, 2));            //The bitRead command tells us what the bit
value is for a specific bit location of a number
        delay(20);                                  //this is needed to make sure the channel switching
event has completed
        Serial3.print("R\r");                       //Poll the port for a value
        sensorstring = Serial3.readStringUntil(13);        //read the string until we see a <CR>
        Serial.print(sensorstring);
        Serial.print(",");                          //Poll the port for a value
        Serial3.print("R\r");                       //Poll the port for a value
        sensorstring = Serial3.readStringUntil(13);        //read the string until we see a <CR>
        Serial.print(sensorstring);
        Serial.print(",C,");
        Serial3.print("sleep\r");
```

```
        sensorstring = Serial3.readStringUntil(13);        //read the string until we see a <CR>
        Serial.print(sensorstring);
        Serial.print(",");

        digitalWrite(s1, bitRead(3, 0));            //Here we have two commands combined into
one.
        digitalWrite(s2, bitRead(3, 1));            //The digitalWrite command sets a pin to 1/0
(high or low)
        digitalWrite(s3, bitRead(3, 2));            //The bitRead command tells us what the bit
value is for a specific bit location of a number
        delay(20);                                  //this is needed to make sure the channel switching
event has completed
        Serial3.print("R\r");                       //Poll the port for a value
        sensorstring = Serial3.readStringUntil(13);        //read the string until we see a <CR>
        Serial.print(sensorstring);
        Serial.print(",");                          //Poll the port for a value
        Serial3.print("R\r");                       //Poll the port for a value
        sensorstring = Serial3.readStringUntil(13);        //read the string until we see a <CR>
        Serial.print(sensorstring);
        Serial.print(",D,");
        Serial3.print("sleep\r");
        sensorstring = Serial3.readStringUntil(13);        //read the string until we see a <CR>
        Serial.print(sensorstring);
        Serial.print(",");

        digitalWrite(s1, bitRead(4, 0));            //Here we have two commands combined into
one.
        digitalWrite(s2, bitRead(4, 1));            //The digitalWrite command sets a pin to 1/0
(high or low)
        digitalWrite(s3, bitRead(4, 2));            //The bitRead command tells us what the bit
value is for a specific bit location of a number
        delay(20);                                  //this is needed to make sure the channel switching
event has completed
        Serial3.print("R\r");                       //Poll the port for a value
        sensorstring = Serial3.readStringUntil(13);        //read the string until we see a <CR>
        Serial.print(sensorstring);
        Serial.print(",");                          //Poll the port for a value
        Serial3.print("R\r");                       //Poll the port for a value
        sensorstring = Serial3.readStringUntil(13);        //read the string until we see a <CR>
        Serial.print(sensorstring);
        Serial.print(",E,");
        Serial3.print("sleep\r");
        sensorstring = Serial3.readStringUntil(13);        //read the string until we see a <CR>
        Serial.print(sensorstring);
        Serial.print(",");
```

```
        digitalWrite(s1, bitRead(5, 0));            //Here we have two commands combined into
one.
        digitalWrite(s2, bitRead(5, 1));            //The digitalWrite command sets a pin to 1/0
(high or low)
        digitalWrite(s3, bitRead(5, 2));            //The bitRead command tells us what the bit
value is for a specific bit location of a number
        delay(20);                                  //this is needed to make sure the channel switching
event has completed
        Serial3.print("R\r");                       //Poll the port for a value
        sensorstring = Serial3.readStringUntil(13);       //read the string until we see a <CR>
        Serial.print(sensorstring);
        Serial.print(",");                      //Poll the port for a value
        Serial3.print("R\r");                       //Poll the port for a value
        sensorstring = Serial3.readStringUntil(13);       //read the string until we see a <CR>
        Serial.print(sensorstring);
        Serial.print(",F,");
        Serial3.print("sleep\r");
        sensorstring = Serial3.readStringUntil(13);       //read the string until we see a <CR>
        Serial.print(sensorstring);
        Serial.print(",");

        digitalWrite(s1, bitRead(6, 0));            //Here we have two commands combined into
one.
        digitalWrite(s2, bitRead(6, 1));            //The digitalWrite command sets a pin to 1/0
(high or low)
        digitalWrite(s3, bitRead(6, 2));            //The bitRead command tells us what the bit
value is for a specific bit location of a number
        delay(20);                                  //this is needed to make sure the channel switching
event has completed
        Serial3.print("R\r");                       //Poll the port for a value
        sensorstring = Serial3.readStringUntil(13);       //read the string until we see a <CR>
        Serial.print(sensorstring);
        Serial.print(",");                      //Poll the port for a value
        Serial3.print("R\r");                       //Poll the port for a value
        sensorstring = Serial3.readStringUntil(13);       //read the string until we see a <CR>
        Serial.print(sensorstring);
        Serial.print(",G,");
        Serial3.print("sleep\r");
        sensorstring = Serial3.readStringUntil(13);       //read the string until we see a <CR>
        Serial.print(sensorstring);
        Serial.print(",");

        digitalWrite(s1, bitRead(7, 0));            //Here we have two commands combined into
one.
        digitalWrite(s2, bitRead(7, 1));            //The digitalWrite command sets a pin to 1/0
(high or low)
```

```
        digitalWrite(s3, bitRead(7, 2));            //The bitRead command tells us what the bit value is for a specific bit location of a number
        delay(20);                                  //this is needed to make sure the channel switching event has completed
        Serial3.print("R\r");                       //Poll the port for a value
        sensorstring = Serial3.readStringUntil(13);     //read the string until we see a <CR>
        Serial.print(sensorstring);
        Serial.print(",");                      //Poll the port for a value
        Serial3.print("R\r");                       //Poll the port for a value
        sensorstring = Serial3.readStringUntil(13);     //read the string until we see a <CR>
        Serial.print(sensorstring);
        Serial.print(",H,");
        Serial3.print("sleep\r");
        sensorstring = Serial3.readStringUntil(13);     //read the string until we see a <CR>
        Serial.print(sensorstring);
        Serial.print(",");

        //Printin out useful stuff here
        Serial.print(float(MaxFlow*sin(i*3.14159/720)),8); //This prints the flow rate during the step
        Serial.print(",");
        Serial.print(float(MaxFlow*sin(i*3.14159/720)*0.5),8); //This prints the volume outputted during the step
        Serial.print(",");
        Serial.print(float(MaxFlow*sin(i*3.14159/720)*0.5/PoreVolume),8);//This prints the pore volume injected during this timestep
        Serial.print(",");
        CycleCumPoreVolume +=MaxFlow*sin(i*3.14159/720)*0.5/PoreVolume;//Adds the new pore volume to the total pore volume in the cycle
        TotalCumPoreVolume +=MaxFlow*sin(i*3.14159/720)*0.5/PoreVolume;//Adds the new pore volume to the total pore volume in the experiment
        TotalVolume += MaxFlow*sin(i*3.14159/720)*0.5;//Adds the new water volume to total volume in the cycle.
        Serial.print(float(CycleCumPoreVolume),8); //This prints the total pore volume for the experiment's cycle
        Serial.print(",");
        Serial.print(float(TotalCumPoreVolume),8);//This prints the total pore volume injected during over the entire experiment
        Serial.print(",");
        Serial.print(float(ExperimentTimer.getValue()/1000),8); //Gets the total timestamp for all looped measurements in seconds
        Serial.print(",");
        Serial.print(float(CycleTimer.getValue()/1000),8); //Gets the total timestamp for this 6hr cycle in seconds
        Serial.print(",");
```

```
        Serial.print(float(LoopTimer.getValue()/1000),8); //Snags the time passed during the loop after measuring the probes in seconds
        Serial.print(",");
        Serial.print(n); //This prints the number for the 12 hr cycle that the experiment is currently on. For example; 2 = second of the 12hr cycles.
        Serial.print(",");
        Serial.print(i); //This prints the 30second timestamp value the column is currently on. For example, 59 = the fifty-nith step.
        Serial.print(",");
        Serial.println(floor((MaxFlow*sin(i*3.14159/720)+A_Intercept)/A_Slope));//This prints out the bit sent to the pump


        while(LoopTimer.getValue()<=LoopTimer.getTimeout()){}
          LoopTimer.stop(); //Stops the loop after exactly 30 second.
          }
   CycleTimer.stop(); //kills the 6hr loop timer
   analogWrite(DAC0,0);
   CycleCumPoreVolume=0;//Wipes the cycle pore volume for the next cycle
   digitalWrite(PumpA,HIGH);//Turns off the pump

   }
   ExperimentTimer.stop();
  while(1==1){}
}
```

Figure B12. This is the code used for calibrating the two peristaltic pumps in the R1D apparatus.

```
#include <RBD_Timer.h>
long TimeStep = 30*1000; //30s in miliseconds
RBD::Timer LoopTimer(TimeStep);

#define Val_1 47
#define Val_2 49
#define Val_3 51

#define PumpA 43
#define PumpB 45

#define AnalogPumpSwap 53

#define PumpMagnitude DAC0
//4:r<CR>

//To open a channel and not send a command just send the channel number followed by a colon.
//1:<CR>
//3:<CR>


String inputstring = "";                    //a string to hold incoming data from the PC
String sensorstring = "";                    //a string to hold the data from the Atlas Scientific
product
boolean input_string_complete = false;              //have we received all the data from the PC
boolean sensor_string_complete = false;              //have we received all the data from the Atlas
Scientific product
String TempCompSTR="";
String TempCompReturn="";

int s1 = 6;                                 //Arduino pin 6 to control pin S1
int s2 = 5;                                 //Arduino pin 5 to control pin S2
int s3 = 4;                                 //Arduino pin 4 to control pin S3
int Counter = 0;
int MAX=6;
int port = 0;
String portstring="";
String DOprobestring="";
int PortNum = 5;


void setup() {
  // put your setup code here, to run once:
  pinMode(Val_1,OUTPUT);
```

```
  pinMode(Val_2,OUTPUT);
  pinMode(Val_3,OUTPUT);
  pinMode(PumpA,OUTPUT);
  pinMode(PumpB,OUTPUT);
  pinMode(AnalogPumpSwap,OUTPUT);
  digitalWrite(Val_1,HIGH);
  digitalWrite(Val_2,HIGH);
  digitalWrite(Val_3,HIGH);
  digitalWrite(PumpA,HIGH);
  digitalWrite(PumpB,HIGH);
  digitalWrite(AnalogPumpSwap,HIGH);
  Serial.begin(9600);                    //Set the hardware serial port to 9600
  Serial3.begin(9600);                    //set baud rate for software serial port_3 to 9600
  inputstring.reserve(10);                //set aside some bytes for receiving data from the PC
  sensorstring.reserve(30);               //set aside some bytes for receiving data from Atlas
Scientific product
  pinMode(s1, OUTPUT);                       //Set the digital pin as output
  pinMode(s2, OUTPUT);                       //Set the digital pin as output
  pinMode(s3, OUTPUT);                       //Set the digital pin as output
  Serial.print("Temperature,EC,pH,ORPMicro,ORP,DO");
  Serial.println();
  analogWriteResolution(12);

}

void loop() {
    delay(10000);
    // 500
    digitalWrite(Val_1,HIGH);
    digitalWrite(Val_2,HIGH);
    digitalWrite(Val_3,HIGH);
    digitalWrite(PumpB,LOW);
    analogWrite(DAC0,500);
    delay(300000);
    analogWrite(DAC0,0);
    digitalWrite(PumpB,HIGH);
    delay(100);

    digitalWrite(Val_1,LOW);
    digitalWrite(Val_2,LOW);
    digitalWrite(Val_3,LOW);
    digitalWrite(PumpA,LOW);
    analogWrite(DAC0,500);
    delay(300000);
    analogWrite(DAC0,0);
    digitalWrite(PumpA,HIGH);
```

```
  delay(100);

  // 1000
  digitalWrite(Val_1,HIGH);
  digitalWrite(Val_2,HIGH);
  digitalWrite(Val_3,HIGH);
  digitalWrite(PumpB,LOW);
  analogWrite(DAC0,1000);
  delay(300000);
  analogWrite(DAC0,0);
  digitalWrite(PumpB,HIGH);
  delay(100);

  digitalWrite(Val_1,LOW);
  digitalWrite(Val_2,LOW);
  digitalWrite(Val_3,LOW);
  digitalWrite(PumpA,LOW);
  analogWrite(DAC0,1000);
  delay(300000);
  analogWrite(DAC0,0);
  digitalWrite(PumpA,HIGH);
  delay(100);

  // 2000
  digitalWrite(Val_1,HIGH);
  digitalWrite(Val_2,HIGH);
  digitalWrite(Val_3,HIGH);
  digitalWrite(PumpB,LOW);
  analogWrite(DAC0,2000);
  delay(300000);
  analogWrite(DAC0,0);
  digitalWrite(PumpB,HIGH);
  delay(100);

  digitalWrite(Val_1,LOW);
  digitalWrite(Val_2,LOW);
  digitalWrite(Val_3,LOW);
  digitalWrite(PumpA,LOW);
  analogWrite(DAC0,2000);
  delay(300000);
  analogWrite(DAC0,0);
  digitalWrite(PumpA,HIGH);
  delay(100);

 while(1==1){}
}
```

APPENDIX C

Detailed Packing Method

Sediment was packed into the column with a modified slurry-pack method. The column was capped at one end and the outlet tubing clipped shut to prevent water flow. The top was left uncapped, and ~200mL of DI water was poured into the column. Air bubbles trapped in the steel baffles in the column bottom were gently excised by repeated percussions with an available crescent wrench. Then, graded sand was gently and slowly poured into the column, allowing the sand to be fully saturated with water, preventing air from being trapped in pore spaces. After ~2-3cm of sand was poured in, the column was gently but firmly tapped on the sides and the top to compact the sand on the bottom of the column. This procedure was repeated until the column was filled with sand at the exact level of the top of the column. Then, the rim of the column and the threads were gently brushed free of sand. Sand grains remaining on the rim or threads can gum up the threads, preventing the caps from sealing and damaging the threads. After the cap was installed, a second clip was placed on the outlet tubing and shut, preventing water from escaping the column. Then, making sure to keep the top of the column the right way up, the column was placed in a holder to keep it vertically oriented. After unclipping the bottom and top clips to briefly flush the tip of the tubing on the bottom the column, the saturated bottom tubing of the column was quickly connected to the apparatus with a barb fitting. Then, the apparatus was programed to perform a 1D flush using DI water to evacuate the last of the air in the top of the column's baffles, fully saturating the column.

Hydraulic Conductivity (K)

Hydraulic Conductivity was measured via a constant head permeameter. In the constant head permeameter test, hydraulic head is kept constant in the apparatus using a funnel that is continually fed with tap water from the sink. The bottom of the funnel feeds into a 3-way stopcock attached to the bottom the monometer and the inlet tube to the permeameter. The inlet tube was attached to the top of the permeameter. The sand was packed into the permeameter following the slurry packing procedure outlined above, resulting in identical packing to the acrylic columns in the apparatus. An outlet tube from the column drained into the sink. For a constant head permeameter test, Darcy's law can be rearranged (Eq. C1)

(Equation C1) $$K = \frac{Q*dl}{A*dh}$$

Where the difference in height between the outlet tube of the column and the top of the funnel was measured (*dh*), the permeameter length (*dl*) was 16cm, the cross-sectional area of the column (*A*) was 31.669 cm, and the flow rate of effluent was (*Q*).

During a constant head permeameter test, the height (h) was recorded. Over a timed interval, water was collected in an Erlenmeyer flask, and the difference between the empty flask mass and the flask+water mass was used to calculate the volume of water by recognizing the density of water at room temperature is 1.00 g/mL. The volume of water divided by the time interval it was collected was the flow rate (Q). The experiment was repeated in triplicate at different heights for each sediment type.

Porosity (n)

Porosity was obtained via bulk density. In this method, a ~50g graded sand sample was administered to an empty graduated cylinder pre-tared on an analytical balance (m_{sand}). The sand was tamped down by tapping the top of the graduated cylinder approximately 20 times, mimicking the packing procedure outlined above. The packed particle volume was then recorded ($V_{sand(dry)}$). The sand was then temporarily dispensed into a beaker on the side. The graduated cylinder was then filled with approximately 60mL of distilled water (V_{water}). Then the sand was readministered to the flask by gently pouring with the aim of preventing air bubbles from being trapped by the sediment. The sand was then gently tapped with a crescent wrench to ensure any residual air bubbles were liberated. The resultant total volume of water and sand was recorded (V_{total}). Porosity was calculated in triplicate using three separate sand samples.

The bulk density of the sand with the pore spaces is equal to sample sediment dry mass divided by sample sediment dry volume, particle density is equal to the mass of the particles divided by their volume, and porosity then can be calculated via (Eqs. 1-3).

(Eq. C2) $$V_{sand} = V_{total} - V_{water}$$

(Eq. C3) $$Particle\ Density = \frac{m_{sand}}{V_{sand}}$$

(Eq. C4) $$Bulk\ Density = \frac{m_{sand}}{V_{sand(dry)}}$$

(Eq. C4) $$n = 1 - \frac{Bulk\ Density}{Particle\ Density}$$

APPENDIX D

Figure D1. Head maps for the column at 0.25 d (D1.1), 0.50 d (D1.2), 0.75 d (D1.3), and 1.00 d (D1.4) are presented, which show the flow reversals that were occurring during the timestep. The lefthand side of the model corresponded to pump B and the righthand side of the column corresponded to pump A.

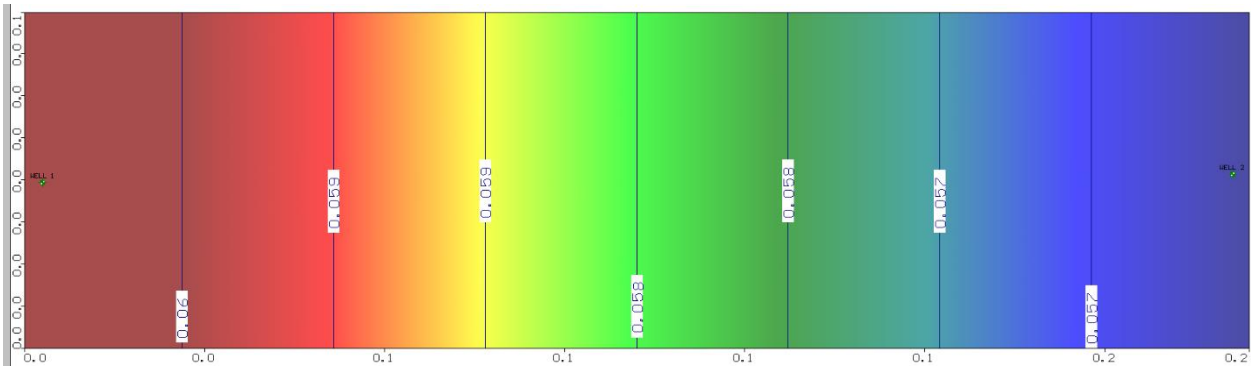

Figure D1.1. This is the head map at timestamp 0.25 d.

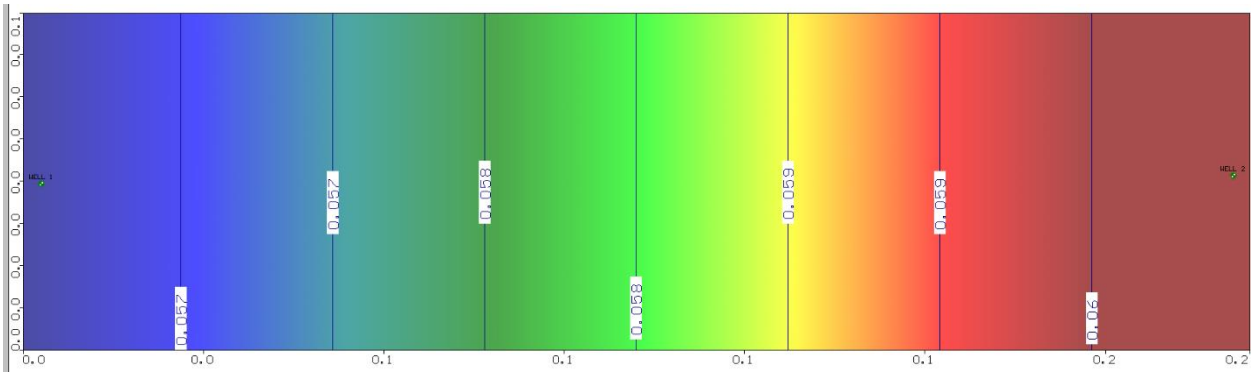

Figure D1.2. This is the head map at timestamp 0.50 d.

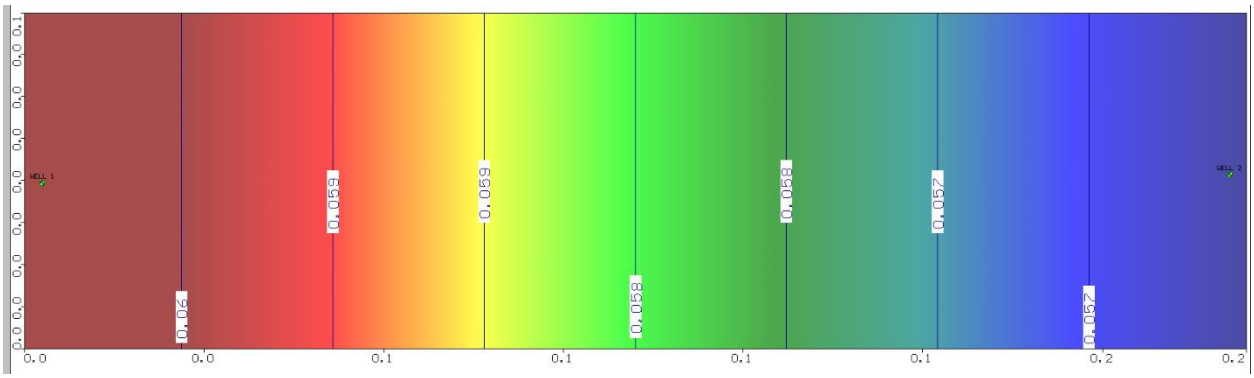

Figure D1.3. This is the head map at timestamp 0.75 d.

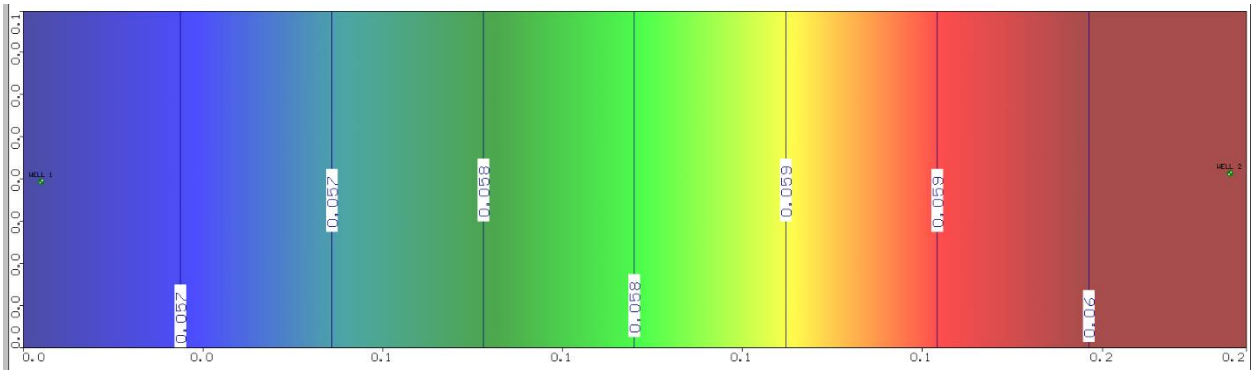

Figure D1.4. This is the head map at timestamp 1.00 d.

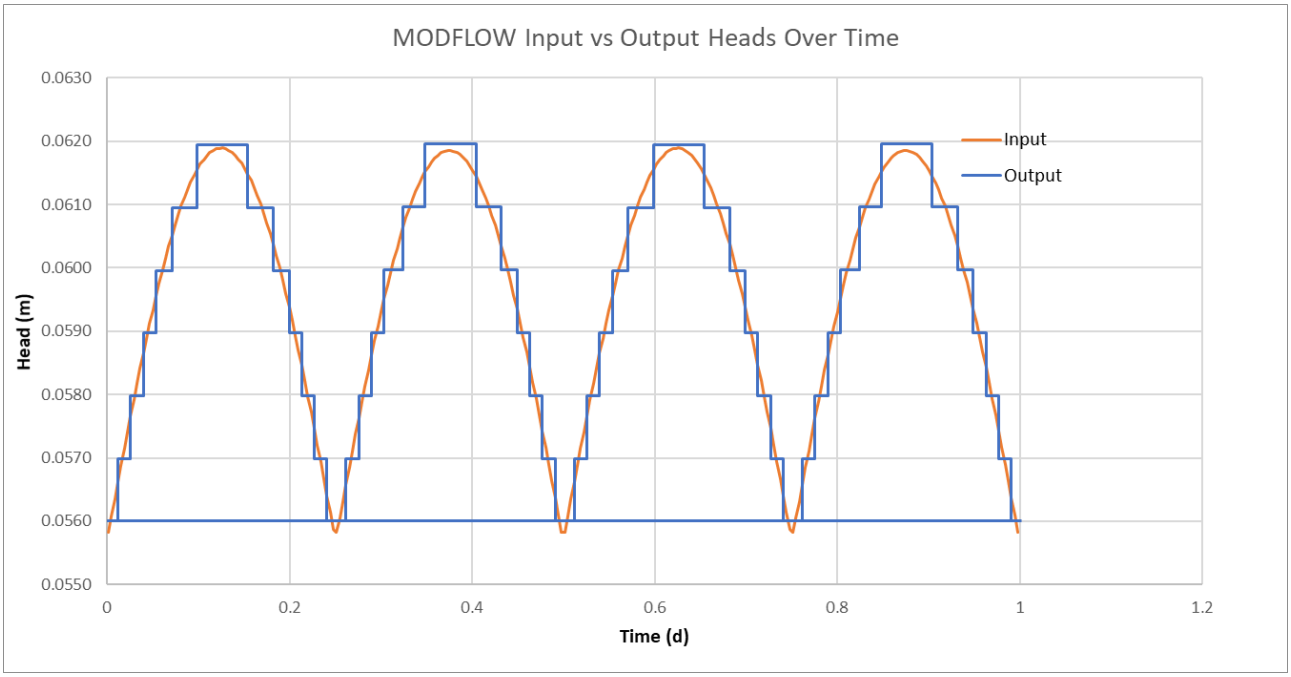

Figure D2. This is a figure presenting the difference between the input heads entered into the mudflow model (orange) and the resultant rounded head values the MODFLOW software used for modeling (blue).